

Interactive comment on Variability of cirrus cloud properties using a Polly^{XT} Raman Lidar over high and tropical latitudes” by Kalliopi Artemis Voudouri et al.

Anonymous Referee #1

The paper presents the results of the cirrus cloud observations performed with a ground-based multi-wavelength PollyXT Raman Lidar during sequential periods between 2008 and 2016, in two subtropical stations (i.e. Gual Pahari in India and Elandsfontein in South Africa) and one subarctic station (i.e. Kuopio in Finland). An automatic cirrus cloud detection algorithm was developed to derive the cirrus cloud lidar geometrical characteristics (cloud boundaries, geometrical thickness) and optical properties (cloud optical depth, lidar ratio, ice crystal depolarization ratio). Then, a statistical analysis and the seasonal variability of these parameters are presented comparing the results of the three sites at different latitudes. The main results of the study are of interest. However, the authors should better characterize these results explaining the scientific context and their novelty and relevancy, re-organizing the structure of the paper that is not well structured. Some sections and figures lack of an accurate description and need to be completed. A more accurate characterization of the developed algorithm used to derive cirrus geometrical and optical properties is required, adding examples and/or references. The discussion of the results, which, in some parts, does not follow a linear path, should be modified giving more emphasis to the comparison among the different stations. The relationships between aerosol load and cirrus optical properties for the three different sites should be considered and discussed in the paper. Furthermore, an added value of this work could be providing an example on how and which the estimated cirrus parameters could be used in the parameterization schemes of the satellite optical retrievals. These issues need to be addressed to better present and to significantly strengthen the results. Thus, I recommend the publication of the manuscript after major revisions, according with the following observations.

We thank the reviewer for his/her remarks that helped us to improve the manuscript. The reviewer is right that parts of the paper should be restructured, as in the present form is not easy to follow the comparisons of the cirrus properties between the different sites. In the revised version the reviewer's comments have been extensively taken into account, by improving the discussion of many sections (i.e., algorithm, comparison among the different stations) and by improving the figures that lacked of an accurate description. Below we report the changes included in the revised manuscript as a response to the comments of the reviewer.

Introduction

1) The introduction lacks of a discussion about cirrus retrievals through CALIOP. Please add some discussions and references.

The reviewer is right. The following text has been added in the revised version.

In the introduction section at page 2-3, we added the following paragraph:

“There are also satellite based studies from either lidar (CloudAerosol Lidar with Orthogonal Polarization (CALIOP), Dupont et al., 2010) or cloud radar (CloudSat) or combined lidar and cloud radar (e.g. Sassen et al. 2008) retrievals that provide a global view concerning the seasonal frequencies of cirrus clouds and their geometrical and optical properties and their variabilities.

However, comparison on cirrus cloud properties performed with ground-based lidar systems for long periods at different geographical locations are scarce, even though that kind of observations that correspond to different areas and atmospheric conditions are crucial to reveal information of the latitudinal dependence of the cirrus properties and indications about the aerosol effect on the geometrical and optical characteristics of the detected cirrus layers. That kind of observations can be further used in the validation of the satellite retrievals, which provide global distribution of cirrus clouds (Sassen et al., 2008). Given that for satellite retrievals, the main input parameter to the optical processing of the cirrus layers is the lidar ratio, the selected lidar ratio value can introduce errors on the retrieved extinction and optical depth values of the cirrus layers, as it is illustrated by Young et al., (2018). The optical depth comparison of the Version 4.10 (V4) of the CALIOP optical depths and the optical depths reported by MODIS collection 6 show substantial improvements relative to earlier comparisons between CALIOP version 3 and MODIS collection 5, as a result of extensive upgrades of the extinction retrieval algorithm. New a priori information of the lidar ratio value for the cirrus layers, included in Version 4.10 (V4) of the CALIOP data products, led to improvements of the extinction and optical depth estimates of the cirrus cloud layers. Thus, ground based lidar observations of the cirrus properties, that correspond to different areas and atmospheric conditions, are crucial to verify and eventually improve the satellite retrievals.

Reference:

Dupont, J.-C., M. Haeffelin, Y. Morille, V. Noël, P. Keckhut, D. Winker, J. Comstock, P. Chervet, and A. Roblin Macrophysical and optical properties of midlatitude cirrus clouds from four ground-based lidars and collocated CALIOP observations, *J. Geophys. Res.*, 115, D00H24, doi:10.1029/2009JD011943, 2010.

Sassen, K., Z. Wang, and D. Liu, Global distribution of cirrus clouds from CloudSat/Cloud-Aerosol Lidar and Infrared Pathfinder Satellite Observations (CALIPSO) measurements, *J. Geophys. Res.*, 113, D00A12, doi:10.1029/2008JD009972, 2008.

Young, S. A., Vaughan, M. A., Garnier, A., Tackett, J. L., Lambeth, J. D., and Powell, K. A.: Extinction and optical depth retrievals for CALIPSO's Version 4 data release, *Atmos. Meas. Tech.*, 11, 5701-5727, <https://doi.org/10.5194/amt-11-5701-2018>, 2018.

2) Lines 61-67, the novelty of the work needs to be discussed and detailed.

The text is modified accordingly and the following sentence is added:

“Ground-based lidar data sets gathered over three sites, two subtropical and one subarctic, are used to evaluate the consistency of cloud geometrical and optical

property climatologies that can be derived by such data sets. The aim of this work is firstly to analyze the cirrus properties over sites in different hemispheres, from observations derived with the same ground based lidar system and secondly to attribute any observable differences to the subarctic and subtropical counterparts. The cirrus properties differences are discussed in order to provide identifications of the possible causes of discrepancies. The study tries to give answers to the following questions:

- Is there a common pattern of the cirrus geometrical and optical properties over different latitudes?
- Can a groundbased lidar system provide.

The analysis presented here could further assist in bridging existing gaps relating to cirrus properties over different regions, since limited long-term cirrus characteristics are available. The information of the lidar ratio is an important parameter for the inversion of lidar signals in instruments that do not have Raman channel and space-based lidars, such as CALIPSO, depend on a parameterization that may vary with location. Thus, information provided by well calibrated ground based measurements is quite critical. Analysis of the lidar ratios values derived from lidar measurements in different parts of the world, where various atmospheric conditions exist will produce results that are more representative of the actual conditions and reductions in the uncertainties related to these lidar ratios will reduce the uncertainties in the retrieved extinction coefficients and derived optical depths.”

3) Section 2, Line 89, please add some details about the nature of the aerosols and their seasonality over the three different sites with appropriate references.

The text is modified accordingly and the following paragraph is added:

“The one year aerosol analysis of lidar observations in Gual Pahari (Komppula et al., 2012) showed that in the summer, the measured air masses were slightly more polluted and the particles were a bit larger than in other seasons (higher Angström exponent values), with the main aerosol sources to be the local and regional biomass and fossil fuel burning. The annual averages revealed a distinct seasonal pattern of aerosol profiles, with aerosol concentrations slightly higher in summer (June – August) compared to other seasons, and particles larger in size. During the summer and autumn, the average lidar ratios were larger than 50 sr, suggesting the presence/dominance of absorbing aerosols from biomass burning. The lidar observations that were performed at Elandsfontein and used for aerosol characterization for the corresponding study period (Giannakaki et al. 2016; Giannakaki et al. 2016) showed that the observed layers were classified as urban/industrial, biomass burning, and mixed aerosols using the information of backward trajectories, MODIS hotspot fire products and in situ aerosol observations. The analysis of the seasonal pattern of vertical profiles of the aerosol optical properties showed that the more absorbing (higher Lidar ratio at 355 nm) biomass particles were larger on August and October, while the category of Urban/industrial had their peak on January, March and May. Another study of the seasonal aerosol climatological characteristics, based on 10 years of MISR data (Tsfaye et al., 2011), showed that the aerosol extinction optical depth

values at 558 nm illustrate annual trends with a maximum during early summer (November–February) and minimum during winter (May–July). Generally, during summer and early winter, the area is dominated by a mixture of coarse-mode and accumulation-mode particles, while during winter and early summer, it is dominated by submicron particles.

Kuopio is an urban area and constitutes a low-aerosol-content environment. The columnar analysis of sunphotometer observations (Aaltonen et al., 2010) revealed that the high Angstrom exponent values observed can be possibly linked with the presence of fine particles, while the seasonal analysis of the optical depth showed that there is no significant variation.”

References:

Aaltonen, Veijo & Rodriguez, Edith & Kazadzis, Stelios & Sogacheva, Larisa & Arola, Antti & de Leeuw, Gerrit.: *Characteristics of the aerosol climatology over Finland based on the optical columnar properties*. 12. 10788, 2010.

Giannakaki, E., van Zyl, P. G., Müller, D., Balis, D., and Komppula, M.: *Optical and microphysical characterization of aerosol layers over South Africa by means of multi-wavelength depolarization and Raman lidar measurements*, *Atmos. Chem. Phys.*, 16, 8109–8123, <https://doi.org/10.5194/acp-16-8109-2016>, 2016.

Giannakaki, E., Pfüller, A., Korhonen, K., Mielonen, T., Laakso, L., Vakkari, V., Baars, H., Engelmann, R., Beukes, J. P., Van Zyl, P. G., Josipovic, M., Tiitta, P., Chiloane, K., Piketh, S., Lihavainen, H., Lehtinen, K. E. J., and Komppula, M.: *One year of Raman lidar observations of free-tropospheric aerosol layers over South Africa*, *Atmos. Chem. Phys.*, 15, 5429–5442, <https://doi.org/10.5194/acp-15-5429-2015>, 2015.

Komppula, M., Mielonen, T., Arola, A., Korhonen, K., Lihavainen, H., Hyvärinen, A.-P., Baars, H., Engelmann, R., Althausen, D., Ansmann, A., Müller, D., Panwar, T. S., Hooda, R. K., Sharma, V. P., Kerminen, V.-M., Lehtinen, K. E. J., and Viisanen, Y.: *Technical Note: One year of Raman-lidar measurements in Gual Pahari EUCAARI site close to New Delhi in India – Seasonal characteristics of the aerosol vertical structure*, *Atmos. Chem. Phys.*, 12, 4513–4524, <https://doi.org/10.5194/acp-12-4513-2012>, 2012.

Tesfaye, M., Sivakumar, V., Botai, J., and Mengistu Tsidu, G.: *Aerosol climatology over South Africa based on 10 years of Multiangle Imaging Spectroradiometer (MISR) data*, *J. Geophys. Res.*, 116, D20216, doi:[10.1029/2011JD016023](https://doi.org/10.1029/2011JD016023), 2011.

Section 3 and Section 4

4) *As the retrieval of optical properties is part of the retrieval algorithm, I would suggest merging Section 3 and Section 4 in three different subsections (3.1, 3.2 and 3.3). The contribution of the background aerosol load to the computation of cirrus cloud products is not negligible. This aspect should be discussed with the appropriate references not only in the last part of the Conclusions but also in this section. Please discuss this point.*

Section 3 and 4 have been merged accordingly. See also comment 3 for the discussion of the background aerosol load. In principal, we assume aerosol free (molecular) region in the altitudes above 6km. The only particles that can act as efficient ice-nucleating particles (INP) at upper tropospheric temperatures are: the dust particles (but usually exist at lower altitudes, Marinou et al., 2019; Ansmann et al., 2019), the volcanic and the aged ice-biomass (e.g., Baars et al., 2019). However, climatological studies in the area, show that these types of aerosols were not present the period studied. For Elandsfontein the upper aerosol layers were found ~3.5km (Giannakaki et al., 2016), while for Gual Pahari the upper layers were below 6km (Komppula et al., 2012) for the period reported in the manuscript.

Ansmann, A., Mamouri, R.-E., Hofer, J., Baars, H., Althausen, D., and Abdullaev, S. F.: Dust mass, cloud condensation nuclei, and ice-nucleating particle profiling with polarization lidar: updated POLIPHON conversion factors from global AERONET analysis, *Atmos. Meas. Tech.*, 12, 4849–4865, <https://doi.org/10.5194/amt-12-4849-2019>, 2019.

Baars, H., Ansmann, A., Ohneiser, K., Haarig, M., Engelmann, R., Althausen, D., Hanssen, I., Gausa, M., Pietruczuk, A., Szkop, A., Stachlewska, I. S., Wang, D., Reichhardt, J., Skupin, A., Mattis, I., Trickl, T., Vogelmann, H., Navas-Guzmán, F., Haefele, A., Acheson, K., Ruth, A. A., Tatarov, B., Müller, D., Hu, Q., Podvin, T., Goloub, P., Vesselovski, I., Pietras, C., Haefelin, M., Fréville, P., Sicard, M., Comerón, A., Fernández García, A. J., Molero Menéndez, F., Córdoba-Jabonero, C., Guerrero-Rascado, J. L., Alados-Arboledas, L., Bortoli, D., Costa, M. J., Dionisi, D., Liberti, G. L., Wang, X., Sannino, A., Papagiannopoulos, N., Boselli, A., Mona, L., D'Amico, G., Romano, S., Perrone, M. R., Belegante, L., Nicolae, D., Grigorov, I., Gialitaki, A., Amiridis, V., Soupiona, O., Papayannis, A., Mamouri, R.-E., Nisantzi, A., Heese, B., Hofer, J., Schechner, Y. Y., Wandinger, U., and Pappalardo, G.: The unprecedented 2017–2018 stratospheric smoke event: Decay phase and aerosol properties observed with EARLINET, *Atmos. Chem. Phys. Discuss.*, <https://doi.org/10.5194/acp-2019-615>, in review, 2019.

Marinou, E., Tesche, M., Nenes, A., Ansmann, A., Schrod, J., Mamali, D., Tsekeri, A., Pikridas, M., Baars, H., Engelmann, R., Voudouri, K.-A., Solomos, S., Sciare, J., Groß, S., Ewald, F., and Amiridis, V.: Retrieval of ice-nucleating particle concentrations from lidar observations and comparison with UAV in situ measurements, *Atmos. Chem. Phys.*, 19, 11315–11342, <https://doi.org/10.5194/acp-19-11315-2019>, 2019.

5) Lines 100-102, please discuss the normalization of signal (step b). How this normalization enhances the method applicability in different atmospheric conditions?

The normalization is applied so as to ensure the applicability of the method (the threshold criteria for cirrus boundaries) to all the lidar systems. Given that lidar signals are uncalibrated and signal levels from one lidar system to another can be rather different, the normalization ensures the applicability of the criteria used by Baars et al., 2008. We normalized the range-corrected signal by its maximum value found below 1500 m. (below 2500 for Elandsfontein), which is usually the maximum value of the range corrected signal within the Boundary Layer, as proposed by Baars (2008), in order to use the same threshold values for the cirrus boundaries.

Baars, H., Ansmann, A., Engelmann, R., and Althausen, D.: Continuous monitoring of the boundary-layer top with lidar, *Atmos. Chem. Phys.*, 8, 7281–7296, <https://doi.org/10.5194/acp-8-7281-2008>, 2008.

6) Lines 113-115, it is not clear to me if the estimated cirrus geometrical and optical parameters are referred to 60-min averages. If yes, it means that, for example, for the cirrus of Fig.2 the detection algorithm will retrieve one cirrus parameter per hour. Is it correct? Please clarify this aspect.

The reviewer is right. The estimated cirrus geometrical and optical parameters are referred to 60-min averages, so the Figure 3 has changed in the revised version of the manuscript, presenting the hourly means profiles.

7) Lines 116- 119, please add more details and references about the criteria a) and c).

The reviewer is right. We also applied an additional one, a threshold temperature to the cirrus top in order to assure that at cloud top no liquid water is present any more and we also changed the one in the cirrus base, so as to enhance the assumption that no liquid is present, as ice formation occurs predominantly via the liquid phase at $T > -27^{\circ}\text{C}$ (Westbrook et al., 2011).

The sentence has been changed to the following:

“Finally, cloud retrievals from the algorithm are classified as cirrus clouds when the following three criteria were met: i) the particle linear depolarization value is higher than 0.25 (Chen et al., 2002; Noel et al., 2002), ii) the altitude is higher than 6km and iii) the base temperature is below -27°C (Goldfarb et al., 2001; Westbrook et al., 2011) and the top temperature is below -37°C (Campbell et al., 2015).”

References:

Campbell, J. R., Vaughan, M. A., Oo, M., Holz, R. E., Lewis, J. R., and Welton, E. J.: Distinguishing cirrus cloud presence in autonomous lidar measurements, *Atmos. Meas. Tech.*, 8, 435– 449, doi:10.5194/amt-8-435-2015, 2015.

Chen, Wei-Nai & Chiang, Chih-Wei & Nee, Jan.: Lidar Ratio and Depolarization Ratio for Cirrus Clouds. *Applied optics*. 41. 6470-6. 10.1364/AO.41.006470, 2002.

Goldfarb, L., Keckhut, P., Chanin, M.-L., and Hauchecorne, A.: Cirrus climatological results from lidar measurements at OHP (44°N , 6°E), *Geophys. Res. Lett.*, 28, 1687–1690, 2001.

Noel, Vincent & Chepfer, Helene & Ledanois, Guy & Delaval, Arnaud & Flamant, Pierre.: Classification of Particle Effective Shape Ratios in Cirrus Clouds Based on the Lidar Depolarization Ratio. *Applied optics*. 41. 4245-57. 10.1364/AO.41.004245, 2002.

Westbrook, C. D., and Illingworth, A. J. (2011), Evidence that ice forms primarily in supercooled liquid clouds at temperatures $> -27^{\circ}\text{C}$, *Geophys. Res. Lett.*, 38, L14808, doi:10.1029/2011GL048021.

8) Lines 143-144, the depolarization condition (particle linear depolarization > 0.25) is used only for Kuopio or also for the other sites? Which is the magnitude of the error/bias introduced by the Rayleigh calibration method? Despite the different calibration method, it could be of interest to show the depolarization ratio values of the other two sites.

Rayleigh calibration could produce large errors on the particle linear depolarization, so we choose to show the climatology of the values only for Kuopio. In the Rayleigh calibration method a very low amount of strong depolarizing aerosols, like dust or ice crystals in the assumed calibration range, causes large errors of the calibration factor and consequently in the particle linear depolarization, as described in detail in Freudenthaler et al. (2009). The error introduced by the Rayleigh calibration, is associated to the reference region assumed, which should be carefully chosen, and can be of the order of 10-40%. Therefore we only used these depolarization ratios only as proxies for the presence of cirrus clouds and we did not show any climatological values, which could be misleading, when compared to the ones accurate calibrated.

Freudenthaler, V., Esselborn, M., Wiegner, M., Heese, B., Tesche, M., Ansmann, A., Müller, D., Althausen, D., Wirth, M., Fix, A., Ehret, G., Knippertz, P., Toledano, C., Gasteiger, J., Garhammer, M., and Seefeldner, M.: Depolarization ratio profiling at several wavelengths in pure Saharan dust during SAMUM 2006, *Tellus B*, 61, 165–179, doi:10.1111/j.1600-0889.2008.00396.x, 2009.

9)Line 156, it might be helpful to clarify the use of the Eloranta model writing the equation of the term $P_1(z)$ of the equation (4) and discussing the assumptions.

The reviewer is right. The equation has changed in the revised version of the manuscript. The model inputs are:

- (i) the laser beam divergence
- (ii) the receiver field of view
- (iii) the cirrus effective radius We use the values given by Wang and Sassen (2002), who had related the effective radius with cirrus cloud temperature.
- (iv) the measured single scattering extinction profile (or the lidar ratio multiplied by the backscatter for the daytime measurements).
- (v) the order of scattering

To calculate the multiple scattering correction, the code applies an iterative method including the following steps:

- i) The measured extinction profile of the cirrus layer is provided.
- ii) With the provided effective radius profile of the cirrus layer (linear relation of the effective radius with the cirrus temperature derived from radio soundings) and the effective (measured) extinction coefficient $\alpha_{\text{par}}(z)$, an iterative procedure provides the ratio $P(z)/P(1)(z)$.
- iii) From (2) a first value for the correcting factor $F(z)$ can be worked out
- iv) The iterative procedure continues till the calculation of a stable correcting factor $F(z)$ is found.
- v) The corrected extinction can be then calculated from equation (5) in the manuscript and hence the value of lidar ratio.

The following sentence has been added in the manuscript: “The model assumes cirrus made up of hexagonal ice crystals and the model inputs are: (i) the laser beam divergence, (ii) the receiver field of view, (iii) the cirrus effective radius, (iv) the measured single scattering extinction profile (or the lidar ratio multiplied by the backscatter for the daytime measurements) and (v) the order of scattering. The estimation of the cirrus effective radius was taken from Wang and Sassen (2002), based on the linear relation of the effective radius with the cirrus cloud temperature derived from radio soundings.”

Section 5

10) The authors decided to present the results for the estimated geometrical and optical cirrus parameters for each site (sub-sections 5.0.2, 5.0.3 and 5.0.4, respectively). In my opinion, this choice makes the discussion of the results confusing. Another choice, which could help the comparison between subtropical and sub-artic sites, could be to divide the results according to geometrical and optical parameters (two sub-sections). This latter option allows both to improve the description and analysis of Fig. 4, Fig.6 and Fig. 7, where the parameters are depicted for all the stations, and to better compare each site. Table 2 should be completed adding also the value of all the other relevant cirrus parameters (e.g. mean/base/top heights, COD, temperature).

The reviewer is right. In the revised version of the manuscript the results are presented according to geometrical and optical parameters and Table 2 and Table 3 have been added with values of the other relevant cirrus properties. The discussion of the section is presented accordingly.

11) Line 172, from Fig. 3 the diurnally variations cannot be observed. Please remove ‘diurnally’ or clarify.

The reviewer is right. The word ‘diurnally’ has been removed in the revised version of the manuscript.

12) Lines 172-176, to analyze if the observed cirrus cover annual pattern is significant, it could be useful to show the number of total measurements per months. Considering your dataset, can you exclude that the observed cirrus cover annual pattern is only an indication of the annual pattern of low clouds/rain? Have you tried to compare this pattern with CALIOP observation over Kuopio region?

Figure shows the pattern of cirrus detection and not the pattern of cirrus occurrence. As Polly^{XT} measures continuously (24/7) under favor weather conditions, indeed the pattern presented here is only an indication and biased by the presence of low clouds and rain. Even though lidars provide information only in rain/low cloud free times, the pattern of seasonality is consistent with satellite retrievals. Concerning the Elandsfontein site, the average seasonal (monthly) dependence of cirrus cloud frequencies from the CLOUDSAT/CALIPSO observations presented by Sassen (2008), follows the same pattern presented in this study.

13) Lines 176-177, could you explain the agreement between cirrus cover and temperature annual pattern? Are there similar results in literature?

The sentence has been rephrased, as it was quite misleading in the previous version of the manuscript. Our purpose was to relate the low water clouds with temperature values and not the cirrus detection. So, now the sentence has been replaced with the following one:

“This monthly pattern of low clouds existence seems to follow the annual temperature cycle over the region (Jylhä et al., 2004), with maximum temperature values observed during the period April to October, while November to February are the coldest months.”

14) Lines 177-179, please add some numbers about the daytime/nighttime cirrus frequency and the number of total measurements. Could you explain these results?

Table 3 in the revised version of the manuscript, 3 shows the number of detected cirrus layer per site and the number of daytime and nighttime measurements and the following sentence has been added:

The following sentences has been added in the revised version of the manuscript: “Table 2 summarizes the mean geometrical values calculated for each site. We can conclude that the differences between the mean values of the geometrical properties in the daytime and nighttime measurements are not statistically significant. “

“Table 3 summarizes the mean optical values discussed above, for the three sites, separating daytime and nighttime observations. Generally, the averaged optical properties values are found to be nearly identical, except one site (New Delhi), where average nighttime optical properties found higher than that of daytime.”

15) Lines 199-201, is this information relevant?

The reviewer is right. The sentence has been removed in the revised version of the manuscript.

16) Line 204, the AOD is referred to the column below the cirrus? Please explain. It could be of interest to relate AOD to cirrus parameters. Could you deepen this aspect?

We apologize, this was a typo (AOD instead of COD). The correlation between AOD and cirrus properties would be a wholly different study. However, we proceed in the calculation of the AOD in the free troposphere, in order to have an indication about the calculated COD and the AOD below cirrus (check the answer to question 23).

17) Lines 204-206 and 229-231, the discussion about Fig.5 is limited to these lines and does not give any relevant element of interest. Furthermore, concerning COD distribution, Sassen and Cho classification provides similar information. Please add some more elements of discussion or remove Fig. 5.

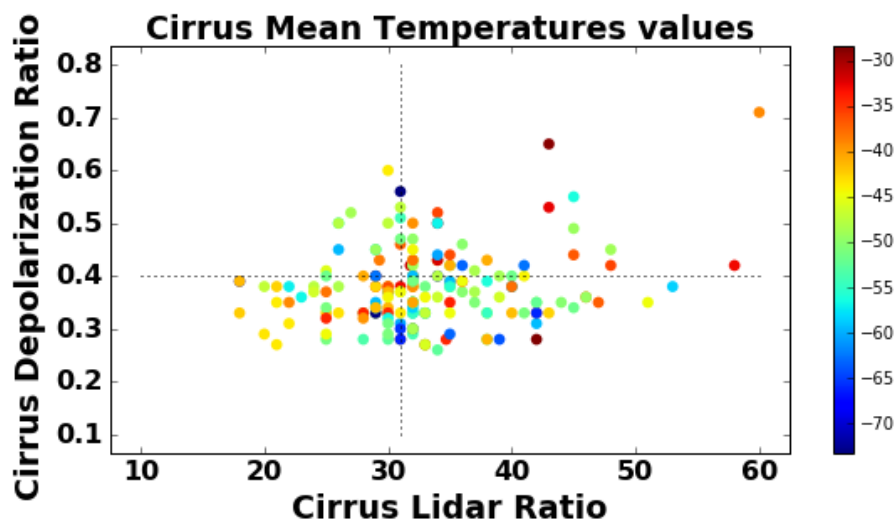
We choose to keep the Figure 7 and to add comments in the results. This figure can provide an evidence that although the lidar dataset is not continuous (due to unfavour weather conditions during winter months), the frequency distributions are representative and even with this scarce sample of data we observe consistent results with other literature studies.

So, we add a paragraph in the revised version of the manuscript:

“To further investigate the distribution of the cirrus lidar ratio values over Kuopio, we present a histogram of the values derived in Fig. 7. The most frequent observed lidar ratio values ranging between 28 and 36 sr for 355 nm and 20 and 36 sr for 532 nm. Similar results have been retrieved regarding the variability of LR 532, which is constant from one month to another, as shown. This figure can provide an evidence that although the lidar dataset are not continuous (due to not favour weather conditions the winter months), the frequency distributions are close to normal and thus the statistics shown here have a significance. In addition we can claim that with this scarce sample of data we observe consistent results with a number of other literature studies.”

18) Lines 216-229, the plot (e) of Fig. 6 is not discussed in the text. Please add some comments. The particle depolarization ratio together with LR and T could help to understand the cirrus crystal composition, size and shape. Did you find some relationship between delta and LR? Please add some comments and, if relevant, some results.

Indeed, the lidar ratio and the depolarization ratio are related to the microphysics and ice compositions of the cirrus clouds and to our knowledge no clear relationship is reported in literature. Concerning our retrievals, the following Figure (Figure 9 in the revised version of the manuscript) shows the relationship between the optical depth and the lidar ratio:



It can be seen from the above, that the highest values of Cirrus lidar ratio (>40) correspond to higher values of Cirrus Depol (>0.4) and warmer cirrus. Moreover, it can be seen the variety of depol values that correspond to the mean value of lidar ratio (~ 31). A similar behavior is reported in Chen et al. (2002).

The following sentence has been added in the revised version of the manuscript:
“The dependency of the mid temperature with the lidar ratio values at 355nm and the particle depolarization values is further examined. Figure 12 shows that the highest values of cirrus lidar ratio (>40) correspond to higher values of cirrus depolarization (>0.4) and warmer cirrus. Moreover, it can be seen the variety of depol values that correspond to the mean value of Lidar Ratio (~ 31). A similar behavior is reported in Chen et al. (2002) for lidar ratio values higher than 30 sr. In his study, the relationship between the depolarization ratio and the lidar ratios shows the former split into two groups for lidar ratios higher than 30. One group has high depolarization ratios about 0.5 and another group has 0.2.”

W. Chen, C. Chiang, and J. Nee, "Lidar ratio and depolarization ratio for cirrus clouds," *Appl. Opt.* 41, 6470-6476, 2002.

19) Line 245, see comment of line 204.

This is a typo, but see also comment on 23.

20) Line 262, see comment of line 204.

This is a typo, but see also comment on 23.

21) Lines 265-269, please add in the discussion the results of the paper of Hoareau et al, 2013, about cirrus measurements at La Reunion sub-tropic site.

The following sentence is added in the revised version of the manuscript:

“Our estimated thickness is slightly smaller than the reported mean value of 2km at La Reunion subtropical region (Hoareau et al., 2012). ” Also the values of their study have been added in Table 5.

Hoareau, C., Keckhut, P., Baray, J.-L., Robert, L., Courcoux, Y., Porteneuve, J., Vömel, H., and Morel, B.: A Raman lidar at La Reunion (20.8° S, 55.5° E) for monitoring water vapour and cirrus distributions in the subtropical upper troposphere: preliminary analyses and description of a future system, Atmos. Meas. Tech., 5, 1333-1348, <https://doi.org/10.5194/amt-5-1333-2012>, 2012.

22) Lines 300-323, this sub-section is of interest and it should be extended. In particular, on the basis of your analyses, is it possible to identify the parameters and the threshold values that could be used in satellite parameterization schemes? How the latitude dependence affect the variability of these parameters?

As latitudinal dependence is found, different parameterization would be necessary to future satellite retrievals. The parameters to be taken into account should be:

- i) the LR value selected for the different counterparts. A latitudinal variation can be seen in the lidar ratios with the lowest values found over the tropical region and over South Africa (Table 2 and Table 3).
- ii) LR values seem to be almost constant between day and night retrievals, except for the Gual Pahari site, where the dataset is not extensive and could not be used as a reference one.

Also Table 3 has been added, summarizing most of the cirrus clouds geometrical and optical properties of ground-based lidar observations reported in literature. Overall, we can conclude that cirrus cloud thicknesses are greatest in the tropics and decrease toward the poles and concerning the lidar ratio values, these seem to be increasing towards the north pole.

The following sentence is added in the revised version of the manuscript:

“The reported values in literature from previous studies based on lidar ground-based dataset and the current one are listed in Table 4. Generally, cirrus layers have been observed up to altitudes of 13km above Gual Pahari, whereas they have only been detected to about 1km lower at the other two regions and this conclusion is in accordance with the Cloudsat observations (Sassen et al., 2008). Based on the satellite information, the derived cirrus cloud thicknesses was found to be larger in the tropics and decreasing toward the poles. Also from the values reported from ground-based studies, a pattern can be concluded: cirrus cloud geometrical properties peaks around the equator and at midlatitudes sites, with generally decreasing amounts as the poles are approached. On the other hand, the lidar ratio values seem to follow a diverse relation, showing greater values moving to the poles. In our study, larger values of LR is found for the subarctic station and smaller LR were observed for Gual Pahari and Elandsfontein.”

23) Line 307, as already mentioned, the relationships between aerosol load and cirrus optical properties should be discussed more in details with a dedicated sub-section. In particular, the aerosol extinction below the cirrus and the type of aerosol could be of interest to understand the role of aerosol in cirrus formation. Do you have any analysis related to this?

Measurement Site	Kuopio	Elandsfontein	Gual Pahari
Type of aerosols	Fine particles	biomass burning aerosols and mixtures of biomass burning aerosols with desert dust	dust particles, biomass burning

		particles and urban/industrial particles	
AOD FT	0.0056 ± 0.009	0.058 ± 0.04	0.0875 ± 0.034
COD	0.25 ± 0.27	0.4 ± 0.3	0.59 ± 0.39

Giannakaki et al. (2016) showed that the aerosol classification over South Africa indicates mostly biomass burning aerosols and mixtures of biomass burning aerosols with desert dust particles, as well as the possible continuous influence of urban/industrial aerosol load in the region.

New Delhi, represents a semi-urban environment surrounded mainly by agricultural test fields and light vegetation. The seasonal characteristics of the aerosol vertical structure performed there (Komppula et al., 2012) indicate the presence of dust particles due to the Asian dust storms.

Kuopio is a semiurban site, where mostly fine particles exist (Aaltonen et al., 2012).

References

Aaltonen, Veijo & Rodriguez, Edith & Kazadzis, Stelios & Arola, Antti & Amiridis, Vassilis & Lihavainen, Heikki & de Leeuw, Gerrit: On the variation of aerosol properties over Finland based on the optical columnar measurements. *Atmospheric Research*. 116. -. 10.1016/j.atmosres.2011.07.014, 2012.

Giannakaki, E., van Zyl, P. G., Müller, D., Balis, D., and Komppula, M.: Optical and microphysical characterization of aerosol layers over South Africa by means of multi-wavelength depolarization and Raman lidar measurements, *Atmos. Chem. Phys.*, 16, 8109–8123, <https://doi.org/10.5194/acp-16-8109-2016>, 2016.

Komppula, M., Mielonen, T., Arola, A., Korhonen, K., Lihavainen, H., Hyvärinen, A.-P., Baars, H., Engelmann, R., Althausen, D., Ansmann, A., Müller, D., Panwar, T. S., Hooda, R. K., Sharma, V. P., Kerminen, V.-M., Lehtinen, K. E. J., and Viisanen, Y.: Technical Note: One year of Raman-lidar measurements in Gual Pahari EUCAARI site close to New Delhi in India – Seasonal characteristics of the aerosol vertical structure, *Atmos. Chem. Phys.*, 12, 4513–4524, <https://doi.org/10.5194/acp-12-4513-2012>, 2012.

24) Line 310, could you explain the choice of using the cirrus base temperature instead of the mean/top temperature as independent parameter?

The reviewer is right that the cirrus base temperature doesn't provide more information and the mean temperature can be more representative of the dependence of geometrical and optical properties. In the revised version of the manuscript all figures have been updated with the mid temperature.

25) Lines 315 and 319, please replace 'Fig.10' with 'Fig. 8'.

As some figures added in the revised version of the manuscript, the order has been changed.

26) Line 321, from Fig.8d the particle depolarization increases is not clear. Is it significant?

Indeed it is not significant. The sentence has been rephrased in the revised manuscript, as follows: “No clear tendency is found, as the variability of this parameter is relatively constant, with a slightly increase of the particle depolarization with the increasing mid temperature”.

Conclusions

27) To summarize the results of this work, it would be useful to add a resuming table that, according to the different latitudes, compares the retrieved cirrus parameters to the main results of the literature reported in the paper.

We thank the reviewer for this comment. Table 5 is added in the revised version of the manuscript, including all the information of the cirrus properties based on ground-based lidar observations reported in the literature for the different latitudes. A latitudinal dependence of the cirrus cloud can be seen. See also answer to question number 22.

The following sentence is added in the revised version of the manuscript:

“The three presented datasets are derived from different latitudinal and climatic sites. In this section we firstly examine the latitudinal dependence of the cirrus geometrical and optical properties. The reported values in literature from previous studies based on lidar groundbased dataset and the retrievals of the current one are listed in Table 5 and plotted in Figure 9 for comparison. We can note, that the cirrus geometrical properties and the lidar ratio values may vary greatly depending on the latitude and an decreasing trend of the geometrical boundaries with the rise of the distance from the equator is obvious, also reported by satellite observations (Sassen et al., 2008). Generally, cirrus layers have been observed up to altitudes of 13km above Gual Pahari, whereas they have only been detected to about 1km lower at the subarctic region and this conclusion is in accordance with the Cloudsat observations (Sassen et al., 2008). Based on the satellite information, the derived cirrus cloud thicknesses was found to be larger in the tropics and decreasing toward the poles. Also from the values reported from groundbased studies, a pattern can be concluded: cirrus cloud geometrical properties peaks around the equator and at midlatitudes sites, with generally decreasing amounts as the poles are approached. On the other hand, the optical properties seem to follow a diverse relation, showing greater values moving to the poles. In our study, larger values of COD 355 and smaller LR were observed for Gual Pahari and Elandsfontein. The larger variability of the optical properties at the two subtropical regions, relative to Kuopio, could be related to the larger and variable aerosol load over these regions.”

Interactive comment on “Variability of cirrus cloud properties using a Polly^{XT} Raman Lidar over high and tropical latitudes” by Kalliopi Artemis Voudouri et al.

Anonymous Referee #2

In the study discussed below, the authors around Kalliopi Artemis Voudouri present a cirrus cloud statistics for several sites where a multi-wavelength Raman lidar system of type Polly-XT was deployed.

The lidar data was analyzed with a newly developed cirrus retrieval algorithm. Cloud boundary detection was based on wavelet transformation of a kind of normalized background-corrected raw signals. For the identified cirrus layers cloud optical properties for 355-nm and 532-nm wavelength were derived and a multiple-scattering correction was applied. The derived statistics of geometrical and optical cirrus cloud properties are diverse.

Clear conclusions could not be drawn.

I see a certain strengths in the manuscript, given the following facts:

- Presentation of a newly developed cirrus cloud identification algorithm*
- Retrieval of Raman-based cirrus optical properties for 355 AND 532 nm*
- Demonstration of the potential of a network of similar Raman lidar systems for application of one single retrieval scheme*

Nevertheless, flaws in the description of the data analysis technique and in the discussion of the statistics dominate my impression while I was reading (several times) through the manuscript. I felt uncomfortable reading through the results section without knowing exactly how the statistics were derived.

“Cases” are presented, but how is one case defined?

See our comment on answer number 13.

To how many cloud profiles was the wavelet transform applied to get the boundaries?

See our comment on answer number 1.

Are the presented optical properties based on Raman or Klett?

See our comment on answer number 11.

These are important questions. Without knowledge about these, the value of the study is very limited.

I thus recommend a major revision of the manuscript, including a second review phase in order to put the study on a more solid footing.

We thank the reviewer for his/her remarks that helped us to improve the manuscript. In the revised version the reviewer’s comments have been extensively taken into account, by improving the discussion of many sections (i.e., algorithm, comparison among the different stations) and by improving the figures that lacked of an accurate description. Moreover, parts of the paper have been restructured and all the figures have been reprocessed, as in the present form is not easy to follow the comparisons of the cirrus properties between the different sites.

Below we report the changes included in the revised manuscript as a response to the comments of the reviewer.

Major comments:

1) 1 – Ch.3; Retrieval Scheme/Fig. 1:

The presentation of a retrieval scheme should always be done in such a way that others are able to reproduce it. The scheme given in Ch. 3 does not allow for that, because important information is missing:

- o Was there range-averaging applied? If yes, under which conditions (see e.g. Fig. 1 b vs. 1 c)*
- o What happened to 1-hour intervals not filled entirely by cirrus clouds?*

How were irregularities in the cirrus cloud structure within the 1-hour averaging period treated?

The reviewer is right that it is difficult to follow the algorithm steps with Figure 2, as the time averaging presented is different. In the revised version of the algorithm however, we reprocessed the data and Figure 3 presents the 1-hour averaged profiles.

To calculate the cirrus boundaries, the code applies the following steps:

- i) The wavelet covariance is calculated for every single profile (every 30s).
- ii) The profiles that fulfil the criteria for a cirrus detection (Figure 2, schematic flowchart) are hourly averaged.
- (iii) A mean value of the cirrus base and top are attributed to the one-hour processing. Nan values (free of cirrus sets) are not computed to the mean boundaries.

We also calculate the differences within an hour between the bases/top calculated for every 30s profile, and these should not exceed the 0.5km. If differences are greater than this value, we exclude the case. With this assumption, we also exclude cases with large variability of cirrus layers.

2) *“the signal is normalized with a maximum value below 1.5km”. What does this mean?*

Was the signal normalized using the maximum value found between the ground and 1.5 km height (or range)?

The normalization is applied to ensure the applicability of the method (the threshold criteria for cirrus boundaries) to all the lidar systems. Given that lidar signals are uncalibrated and signal levels from one lidar system to another can be rather different, the normalization ensures the applicability of the criteria used by Baars et al., 2008. We normalized the range-corrected signal by its maximum value found below 1500 m. (below 2500 for Elandsfontein), which is usually the maximum value of the range corrected signal within the Boundary Layer, as proposed by Baars (2008), in order to use the same threshold values for the cirrus boundaries.

3) *In Eq. (1): What is z? altitude or range? Is this z the same z as the one in Eq. 3?*

I fear that range and height are mixed-up somewhat. Introduce separate variables for height and range where applicable/needed. Also: Is altitude above ground or above sea level (asl)? Was this considered in the statistics (given that the station elevation varies from 190 to 1745 m asl)?

Yes, the altitude in all plots corresponds to height above sea level, and this is considered in the statistics.

4) *Eq. 2: What is Csig? Raw signal? Counts? What is Cbg? What is the difference between C and P (Eq. 1 vs. Eq. 2)?*

C stands for the lidar raw signal, while P is the signal after applying the SNR filter, the background correction, the range correction and the normalized correction. That is the reason for using different symbols.

5) Case study/Fig. 2: The case study spans over about 4 hours, but the standard averaging period to derive the wavelet and particle depolarization ratio was 1 hour, wasn't it? I propose to show a case study that uses the actual time- and range-resolution used in the cirrus retrieval scheme.

The reviewer is right. In the revised version of the paper we revised Figure 3, with the hourly application of the cirrus retrieval scheme to the case study.

6) According the Figure 1, zero and background levels as well as normalization were applied to the range-corrected signal. Is this true? Shouldn't at least the background and zero values be subtracted from the raw signal?

We firstly applied the threshold for the SNR, we then corrected the signal for the zero and background, we calculated the range corrected signal and finally, we applied the wavelet.

7) The selected base temperature of $<-20^{\circ}\text{C}$ (see Fig. 1) gives risk to the inclusion of layers of supercooled liquid water into the statistics, as ice formation occurs pre-dominantly via the liquid phase at $T<-27^{\circ}\text{C}$ (Westbrook et al., 2011). Was there any threshold put on the temperature at cloud top? I'd believe a good value for this could be -38°C or so in order to assure that at least at cloud top no liquid water was present any more.

The reviewer is right. In the revised version of the manuscript we applied an additional criteria for classification, regarding the top temperature in our data processing. So, in Figure 2 the schematic flowchart has been changed with the new threshold applied to the top temperature and also all figures have been reprocessed, according to this new value.

We also modified the paragraph in the revised version, which now reads: "Finally, cloud retrievals from the algorithm are classified as cirrus clouds when the following four criteria were met: i) the particle linear depolarization value is higher than 0.25 (Chen et al., 2002; Noel et al., 2002), ii) the altitude is higher than 6km and iii) the base temperature is below -27°C (Goldfarb et al., 2001; Westbrook et al., 2011) and iv) the top temperature is below -38°C (Campbell et al., 2015)."

Campbell, J. R., Vaughan, M. A., Oo, M., Holz, R. E., Lewis, J. R., and Welton, E. J.: Distinguishing cirrus cloud presence in autonomous lidar measurements, *Atmos. Meas. Tech.*, 8, 435– 449, doi:10.5194/amt-8-435-2015, 2015.

8) In Fig. 1: Again, what is altitude? Above sea level?

Yes, the altitude corresponds to altitude above sea level.

9) In Fig. 1: Particle linear depolarization ratio is used as criteria for cirrus classification. But this parameter requires the detection of particle backscatter coefficient first.

Shouldn't Fig. 1 thus contain an additional column (between CWT and cirrus criteria) that describes the calculation of the optical properties and multiple-scattering correction?

Yes, the reviewer is right. We revised Figure 3, with the hourly application of the cirrus retrieval scheme to the case study and we also added the hourly backscatter profile.

10) In Fig. 2: Why do the cloud boundaries differ between (b) and (c)? Was there vertical smoothing applied to (c)?

Yes, they differ due to the different time averaging and also to the smoothing applied to the optical properties. In the revised version of the manuscript, we changed smoothing to more strict ones and we reprocessed the figure with the hourly application of the wavelet and the hourly retrievals.

11) - Cirrus optical properties:

- During daytime, Klett-Fernald was applied, and during nighttime Raman was applied?

Which values went into the statistics of lidar ratio, optical depth and particle depolarization ratio? Both? Only nighttime?

Yes, the reviewer is right. Both values from the two methods are presented in the statistics presented. However, in the revised version, Table 2 and Table 3 have been added, giving the information of the different geometrical and optical values derived from the two methods. See also comment on answer 13.

12) How were reference height and values determined/set?

The determination of the reference height range in the PollyXT software, is made as follows (Baars et al., 2016):

- the user determines the reference height range (zref) from the quicklook of the range corrected signal and provides the sounding file.
- the code calculates the Rayleigh fits (Freudenthaler, 2009) for several zref
- assesses the determined zref
- finds the optimum zref

A similar method is applied in the Single Calculus Chain algorithm for the backscatter calibration (Mattis et al., 2016). In this method, it is also assumed that the height range provided by the user, where the signal or signal ratio has its minimum is closest to the assumed particle-free conditions.

Baars, H., Kanitz, T., Engelmann, R., Althausen, D., Heese, B., Komppula, M., Preißler, J., Tesche, M., Ansmann, A., Wandinger, U., Lim, J.-H., Ahn, J. Y., Stachlewska, I. S., Amiridis, V., Marinou, E., Seifert, P., Hofer, J., Skupin, A., Schneider, F., Bohlmann, S., Foth, A., Bley, S., Pfüller, A., Giannakaki, E., Lihavainen, H., Viisanen, Y., Hooda, R. K., Pereira, S. N., Bortoli, D., Wagner, F., Mattis, I., Janicka, L., Markowicz, K. M., Achtert, P., Artaxo, P., Pauliquevis, T., Souza, R. A. F., Sharma, V. P., van Zyl, P. G., Beukes, J. P., Sun, J., Rohwer, E. G., Deng, R., Mamouri, R.-E., and Zamorano, F.: An overview of the first decade of Polly^{NET}: an emerging network of automated Raman-polarization lidars for continuous aerosol profiling, *Atmos. Chem. Phys.*, 16, 5111–5137, <https://doi.org/10.5194/acp-16-5111-2016>, 2016.

Freudenthaler, V.: Lidar Rayleigh-fit criteria, in: EARLINET-ASOS 7th Workshop, available at: <http://nbn-resolving.de/urn/resolver.pl?urn=nbn:de:bvb:19-epub-12970-6> (last access: 11 February 2015), 2009.

Mattis, I., D'Amico, G., Baars, H., Amodeo, A., Madonna, F., and Iarlori, M.: EARLINET Single Calculus Chain – technical – Part 2: Calculation of optical products, *Atmos. Meas. Tech.*, 9, 3009–3029, <https://doi.org/10.5194/amt-9-3009-2016>, 2016.

13) In the results section, there should be a discussion of Klett-vs-Raman-based results.

Table 2 in the revised version of the manuscript, shows the average cloud base and top altitudes and the average geometrical thickness for each site separating daytime and nighttime measurements. The averaged geometrical properties are found to be nearly identical above all sites, with differences less than 0.2km. Table 3 shows the averaged lidar ratio values, which found to be nearly identical above all except Gual Pahari site where average nighttime LR is 4sr higher than that of daytime.

“Table 2 summarizes the mean geometrical values calculated for each site. Differences between the mean values of the geometrical properties in the daytime and nighttime measurements are less than 200m for all sites.”

“Table 3 summarizes the mean optical values discussed above, for the three sites, separating daytime and nighttime observations. Generally, the averaged optical properties values are found to be nearly identical, except one site (New Delhi), where average nighttime optical properties found higher than that of daytime. But since this dataset is limited, it cannot be used as a reference one.”

14) - Ch 4.02 Multiple Scattering correction:

- The lidar observations provide P_{tot} , but P_1 is required. Eq. 4 thus contains 2 unknowns: P_1 , and $F(z)$. How could the authors solve this equation?

To calculate the multiple scattering correction, the code applies an iterative method including the following steps:

- i) The measured extinction profile of the cirrus layer is provided.
- ii) With the provided effective radius profile of the cirrus layer (linear relation of the effective radius with the cirrus temperature derived from radio soundings) and the effective (measured) extinction coefficient $\alpha_{par}(z)$, the model provides the ratio $P(z)/P(1)(z)$.
- iii) From (2) a first value for the correcting factor $F(z)$ can be worked out.
- iv) The iterative procedure continues till the calculation of a stable correcting factor $F(z)$ is found.
- v) The corrected extinction can be then calculated from equation (5) in the manuscript and hence the value of lidar ratio.

15) - Ch. 5.01 Cirrus cloud cover detection:

- How is a case defined? What does it mean if there were 28 cases observed over Kuopio in April (P7, L175)?

A case is defined as an hourly case. The algorithm searches every set and the ones that fulfill the criteria for cirrus detection, are hourly averaged. See also comment on question 1.

16) Table 2: What is N? Are these the number of hourly samples?

Yes, these are numbers of hourly samples.

17) – Ch. 5.05:

The title can be modified to 'cirrus classification at Kuopio' because the section only deals with this site.

The reviewer is right. In the revised version of the manuscript this paragraph has been changed and the title of the Section 4.0.4 is "Cirrus classification at Kuopio".

18) – Ch. 5.06, Line 321:

Could the decrease of particle LDR with increasing temperature be explained by the sporadic presence of supercooled liquid water?

Generally, the decreasing particle LDR with increasing temperature is believed to reflect the gradual change in basic ice crystal shape, from plates to columns (Noel et al., 2002). Weitkamp also reported that the presence of supercooled water droplets in cirrus is uncommon. Maybe a combination of cloud radar and lidar retrievals can give as more information.

Lidar. Range-Resolved Optical Remote Sensing of the Atmosphere, in the Springer Series in Optical Sciences, edited by Claus Weitkamp

19) - Conclusions:

- What conclusion can be drawn on the conversion of cirrus optical properties from 532 nm to 355 nm, considering that such conversion factors might be required to make future 355-nm/532-nm spaceborne lidar observations comparable? Can the authors make suggestions on which aspects future studies should look in more detail?

The assumption that the backscatter and the extinction coefficients for sufficiently large cirrus particles are spectrally independent; that is, the ratio of cloud backscatter coefficients and the ratio of cloud extinction coefficients will both equal unity, is well established (Reagan et al, 2002) and used in satellite processing schemes. But, it is also reported that the measured variability of cirrus color ratios is much larger than previously realized and that measured color ratios are higher in the tropics (Vaughan et al., 2010). From this study, mean values of LR and COD values in Figure 3 can indicate that there is not a significant spectral dependence, derived from groundbased dataset and differences are mainly found to the extinction profiles (also reported by Haarig et al. 2016). Reasons for that deviations could be either an increase in the MS effect with decreasing wavelength, or that the cirrus crystal size distribution could cause stronger extinction at 532 than at the shorter wavelength of 355 nm, or to the different saturation inside the cirrus layer. Figure 11 presenting the color ratios values on 5°C intervals of cirrus mid temperature, indicate an almost stable behavior with temperature. Generally, we can conclude that for higher altitudes, lower spectral dependence is noticed, taking also into account the number of measurements performed at each site. For the Kuopio station, mean BAE is found 1.1 ± 0.9 , while for the less extensive dataset of New Delhi the mean value is found 1.5 ± 0.8 and for Elandsfontein the mean value is 1.4 ± 1.1 . So, maybe a more representative dataset in the tropics, should be used in order to conclude about the spectral dependence in these regions.

Reagan, J. A., X. Wang, and M. T. Osborn, Spaceborne lidar calibration from cirrus and molecular backscatter returns, IEEE Trans. Geosci. Remote Sens., 40, 2285–2290, 2002.

Vaughan, M. A., Liu, Z., McGill, M. J., Hu, Y., and Obland, M. D., On the spectral dependence of backscatter from cirrus clouds: Assessing CALIOP's 1064 nm calibration assumptions using cloud physics lidar measurements, J. Geophys. Res., 115, D14206, doi:[10.1029/2009JD013086](https://doi.org/10.1029/2009JD013086), 2010.

In addition to the points addressed above, I recommend a thorough peer-review of spelling and grammar by the co-authors in beforehand to the submission of the revised manuscript.

- Minor comments will be addressed in the revised version.

References:

Westbrook, C. D., and Illingworth, A. J. (2011), Evidence that ice forms primarily in supercooled liquid clouds at temperatures > -27 ° C, Geophys. Res. Lett., 38, L14808, doi:10.1029/2011GL048021.

Variability of cirrus cloud properties using a Polly^{XT} Raman Lidar over high and tropical latitudes.

Kalliopi Artemis Voudouri¹, Elina Giannakaki^{2,3}, Mika Komppula³, and Dimitris Balis¹

¹Laboratory of Atmospheric Physics, Physics Department, Aristotle University of Thessaloniki, Greece

²Department of Environmental Physics and Meteorology, Faculty of Physics, University of Athens, Greece

³Finnish Meteorological Institute, P.O.Box 1627, FI-70211, Kuopio, Finland

Correspondence: Kalliopi Artemis Voudouri (kavoudou@physics.auth.gr)

Abstract. Measurements of ~~cirrus clouds~~ geometrical and optical properties of cirrus clouds, performed with a multi-wavelength Polly^{XT} Raman Lidar, during the period 2008 to 2016 are analysed. The measurements were performed with the same instrument, during sequential periods, in three places at different latitudes, Gual Pahari (28.43°N, 77.15°E, 243m a.s.l) in India, Elandsfontein (26.25°S, 29.43°E, 1745m a.s.l) in South Africa and Kuopio (62.74°N, 27.54°E, 190m a.s.l) in Finland. The

5 lidar dataset has been processed by an automatic cirrus cloud ~~detection algorithm~~ masking algorithm, developed in the frame of this work. In the following, we present a statistical analysis of the lidar ~~derived~~ retrieved geometrical characteristics (cloud boundaries, geometrical thickness) and optical properties of cirrus clouds (cloud optical depth, lidar ratio, ice crystal depolarization ratio) measured ~~in different latitudes over the three areas~~ that correspond to subtropical and subarctic regions as well as, their seasonal variability. The effect of multiple-scattering from ice particles to the derived optical products is also

10 considered and corrected in this study. Our results show that ~~, over the subtropical stations,~~ cirrus layers, which have a noticeable monthly variability, were observed between ~~7-6.5~~ to 13km, with ~~mid-cloud~~ temperatures ranging from ~~-60-72~~ °C to -21-27°C. The observed differences on cirrus clouds geometrical and optical properties over the three regions are discussed in terms of latitudinal and temperature dependence. The latitudinal dependence of the geometrical properties is consistent with satellite observations, following the pattern observed with CLOUDSAT, with decreasing values towards the poles. Generally

15 the geometrical boundaries have their highest values in the subtropical regions and overall, our results seem to demonstrate that subarctic cirrus clouds are colder, lower, and a mean thickness of $1295 \pm 489\text{m}$ and $1383 \pm 735\text{m}$ for Gual Pahari and Elandsfontein respectively. The corresponding overall mean cirrus optical depth at 355nm is calculated to be 0.59 ± 0.39 and 0.40 ± 0.33 , with lidar ratio values at 355nm of 26 ± 12 sr and 25 ± 6 sr, respectively. A more extended dataset was acquired for the subarctic area of Kuopio Finland, between 2012 and 2016. The estimated average geometrical thickness of the cirrus

20 clouds over Kuopio is $1200 \pm 585\text{m}$ and the temperature values vary from -71 optical thinner than subtropical cirrus clouds. The dependence of cirrus clouds geometrical thickness and optical properties on mid temperature shows quite similar tendency for the three sites, but less variability for the subarctic dataset. Cirrus are geometrical and optical thicker at temperatures between -45°C to -21 and -35°C and a second peak is observed at lower temperatures $\sim -70^\circ\text{C}$, while the mean cirrus optical depth at 355nm is 0.25 ± 0.2 , with an estimated mean lidar ratio of 33 ± 7 sr, similar to the lidar ratio values observed over middle

25 latitude stations for the subarctic site. Lidar ratio values also exhibit a pattern, showing higher values moving to the poles, with

higher mean value observed over the subarctic site. The dependency of the mid temperature with the lidar ratio values and the particle depolarization values is further examined. Our study shows that the highest values of cirrus lidar ratio correspond to higher values of cirrus depolarization and warmer cirrus. The kind of information presented here can be rather useful in the cirrus parameterizations required as input to radiative transfer models, and can be a complementary tool to satellite products that cannot provide cloud vertical structure. In addition, a-ground-based statistics of the cirrus properties could be useful in the validation and improvement of the corresponding derived products from satellite retrievals.

Copyright statement. TEXT

1 Introduction

Cirrus clouds are usually formed in altitudes from 5-6 to 14km, having an average thickness of 1.5km and temperature variability from -80°C to -20-27°C (Westbrook et al., 2011). Cirrus are made predominantly, or entirely, of ice particles and the shape of their hydrometeors varies, affected by air temperature, atmospheric pressure, and ice supersaturation (Lynch et al., 2001). Given that cirrus clouds are challenging components in atmospheric and global climatological research, affecting the global radiation budget (e.g. Campbell et al., 2016), a number of studies have been focused on quantifying their geometrical, optical and microphysical properties (e.g. Seifert et al., 2007; Dionisi et al., 2013; Pandit et al., 2015). Furthermore, As systematic monitoring and accurate characterization of cirrus properties are important in the evaluation of models and satellite retrievals and, a detailed monitoring of their properties at different geographical locations is crucial to understand their effects on climate.

Active remote sensing techniques, such as lidar and cloud radar instruments, have proved to be useful tools in providing continuous monitoring of high spatial and temporal distributions of cirrus clouds boundaries and their properties, and thus, enhancing the opportunity of tracking cloud evolution both in time and in height. The capability of a cloud radar to map vertical and temporal structures of cloud layers has already been well recognized in the scientific community (Illingworth et al., 2007). Additionally, elastic backscatter and Raman lidars have also been used for retrieving geometrical and optical properties of cirrus clouds (i.e., Ansmann et al., 1992; Gouveia et al., 2017). Moreover, portable multiwavelength lidars (Polly^{XT}) allow for 24/7 monitoring of the atmospheric state (Engelmann et al., 2016) and can be used to establish long time series of aerosol or cloud measurements. Lidar observations also allow the retrieval of detailed hydrometeor properties, such as their sphericity, which is indicative of the shape of targets. The importance of ground-based lidar in monitoring cirrus clouds, is based on the mapping of particularly optically thin high altitude ice clouds which cannot produce sufficient reflectivity and as a consequence can be undetectable from cloud radars (Comstock et al., 2002) or from passive instruments. However, lidar beam attenuates effectively strongly in liquid water clouds, and therefore, it is likely that in the case of multiple cloud layers reliable detection of cirrus clouds cannot be ensured.

In the last decades, ~~efforts of~~ observations of cirrus clouds properties have been conducted both in terms of field experiments (e.g. Seifert et al., 2007) and systematic observations (e.g. Dionisi et al., 2013; Pandit et al., 2015) ~~, in order to estimate from groundbased lidar systems, providing an estimation of~~ their dependence on the geographical location. Dionisi et al. (2013) presented a methodology for identification and characterization of cirrus clouds properties, applied to the multiwavelength Rayleigh ~~Mie??Raman~~ Mie-Raman (RMR) lidar in Rome. The study classified the detected cirrus clouds in different categories, based on their optical properties. Specifically, the analysis showed that 10% of the detected cirrus were subvisible clouds ($\tau < 0.03$), 49% thin ($0.03 < \tau < 0.3$) and 41% opaque cirrus ($\tau > 0.3$). The overall mean value of cirrus optical depth was calculated 0.37 ± 0.18 , while the mean LR_{eff_eff} value was 31 ± 15 sr. Another statistical analysis on optical and geometrical properties of upper-tropospheric cirrus clouds based on a lidar dataset, was conducted in Amazonia (Gouveia et al., 2017). The frequency of occurrence of cirrus clouds classified as subvisible was 41.6%, whilst 37.8% was for thin cirrus and 20.5% for opaque cirrus. The correction of the multiple scattering effect to the optical products in this study was made following the model of Hogan (2008). Lakkis et al. (2015) revealed that the most commonly observed cirrus were characterized as optically thin cirrus, rather than opaque ones, with a mean optical depth value of 0.26 ± 0.11 , over Buenos Aires ($34.6^{\circ}S$, $58.5^{\circ}W$). ~~Nevertheless, comparison on cirrus cloud properties performed with~~ There are also satellite based studies from either lidar (Cloud-Aerosol Lidar with Orthogonal Polarization (CALIOP), Dupont et al., 2010) or cloud radar (CloudSat) or combined lidar and cloud radar (e.g. Sassen et al. 2008) retrievals that provide a global view concerning the seasonal frequencies of cirrus clouds and their geometrical and optical properties and their variabilities.

~~However, there are only few long-term studies based on ground-based lidar systems for long periods at different geographical locations are scarce. However,~~ while these have a limited geographical distribution. This kind of observations that correspond to different areas and atmospheric conditions are crucial to reveal information of the latitudinal dependence of the cirrus properties and can provide indications about the aerosol effect on the geometrical and optical characteristics of the detected cirrus layers. That kind of On top of that, these observations can be further used in the validation and improvement of the satellite retrievals, which provide global distribution of cirrus clouds (Sassen et al., 2008). Given that for satellite retrievals, the main input parameter to the optical processing of the cirrus layers is the lidar ratio, the selected lidar ratio value can introduce errors on the retrieved extinction and optical depth values of the cirrus layers, as it is illustrated by Young et al., (2018). The optical depth comparison of the Version 4.10 (V4) of the CALIOP optical depths and the optical depths reported by MODIS collection 6 show substantial improvements relative to earlier comparisons between CALIOP version 3 and MODIS collection 5, as a result of extensive upgrades of the extinction retrieval algorithm. New apriori information of the lidar ratio value for the cirrus layers, included in Version 4.10 (V4) of the CALIOP data products, led to improvements of the extinction and optical depth estimates of the cirrus cloud layers. Thus, ground based lidar observations of the cirrus properties, that correspond to different areas and atmospheric conditions, are crucial to verify and eventually improve the satellite retrievals.

The aim of this work is ~~firstly to provide cirrus geometrical and optical properties in different hemispheres, based on ground-based lidar data and secondly to attribute any observable differences of cirrus properties to the subarctic and subtropical counterparts, to retrieve and analyze the cirrus geometrical, intensive and extensive optical properties at different latitudes (subtropical and subarctic), from observations derived with the same ground based lidar system, which partly fills the gap~~

concerning the latitudinal coverage of existing ground-based lidar studies. Then the observed differences are discussed in order to identify the possible causes. The information of the lidar ratio is an important parameter for the inversion of lidar signals in instruments that do not have Raman channel and space-based lidars, such as CALIPSO, and depend on a parameterization that may vary with location. Thus, information provided by well-calibrated ground based measurements is quite critical. Analysis of the lidar ratios values derived from lidar measurements in different parts of the world, where different atmospheric and aerosol conditions prevail, will provide results that are more representative of the actual conditions and thus their use will lead to reductions in the uncertainties of the satellite retrievals.

The manuscript is structured as follows: after a brief description of the portable lidar system (Polly^{XT}) and the measuring sites in Section 2, we present the data analysis algorithm in Section 3. Section 4 describes and the methods applied for the optical products retrievals. A in Section 3. The lidar derived statistical analysis and seasonal variations of geometrical and optical properties of cirrus clouds in both subtropical and subarctic areas over the period 2008-2016 is presented and discussed in Section 5.4. Concluding remarks are presented in Section 6.5.

2 Instrument and Measuring Sites

A multi-wavelength depolarization Raman lidar Polly^{XT} of the Finnish Meteorological Institute (FMI) performed automated measurements during the period 2008-2016 in three different geographical regions. The system is based on a compact, pulsed Nd:YAG laser, emitting at 355, 532 and 1064 nm, at 20 Hz repetition rate. The laser beam is pointed into the atmosphere at an off-zenith angle of 5°, so the impact of the specular reflection by ice crystals into cirrus layers on the backscattered signals is negligible. The backscattered signal is collected by a Newtonian telescope, with 0.9m focal length. The vertical resolution of the signal profiles is equal to 30m and the temporal resolution is 30s. The setup of the system includes two Raman channels at 387 and 607 nm, three elastic channels at 355, 532 and 1064 nm, a depolarization channel at 355nm (for India and South Africa), a water vapour channel at 407nm and depolarization channel at 532nm (cross-polarization-cross-polarization with respect to the initial emitted polarization plane) for Kuopio. Detailed description of the system is provided in Althausen et al., 2009 and Engelmann et al., 2015. All measurements processed within the period 2008-2016 are available online at <http://polly.tropos.de>. A more detailed description of the system components is presented in Table 1.

The Polly^{XT} has participated in two campaigns in two subtropical areas, within the framework of the EUCAARI (European Integrated project on Aerosol Cloud Climate and Air Quality interactions) project (Kulmala et al., 2011), covering a wide range of cloud types. Measurements have been performed in Gual Pahari (28.43°N, 77.15°E, 243m a.s.l) in India from March 2008 to March 2009 (Komppula et al., 2012), and in Elandsfontein (26.25°S, 29.43°E, 1745m a.s.l) about 150km from Johannesburg in South Africa from December 2009 to January 2011 (Giannakaki et al., 2015). The measurements Figure 1 presents the map of the three measuring sites. Measurements in Gual Pahari were not performed continuously from March 2008 to March 2009. Due to technical problems with the laser, the data coverage from September to January was limited. Measurements could not be done in October 2008 and January 2009, and in September and November-December only a few usable profiles were measured (Komppula et al., 2012). Measurements in Elandsfontein were performed almost continuously, as two periods were dedicated

to the maintenance of the system (the one from December ~~23rd~~ 23rd to January 26th 2009 and the second one, from October
 125 23rd to November ~~23rd~~ 23rd 2010). Since November 2012 the Polly^{XT} is operating in Kuopio (62.74° N, 27.54° E, 190m a.s.l.)
 in Finland providing continuous measurements and information for the presence of clouds of the subarctic area (Filioglou et al,
 2017). The three measurement sites constitute regions with different atmospheric conditions and different ~~nature and~~ sources
 of aerosol ~~-Evaluation of this and evaluation of the~~ cirrus dataset in ~~various these~~ latitudinal experimental sites ~~will provide~~
~~provides~~ valuable information of the regional characteristics of the measured cirrus properties.

130 3 ~~Description Geometrical and optical retrievals of the cirrus retrieval algorithm~~ clouds

3.1 ~~Description of the cirrus retrieval algorithm~~

Several steps were followed for the processing of the ~~range-corrected~~ signal at 1064nm derived by the Polly^{XT}, needed for the
 estimation of the cirrus boundaries. These are illustrated in Figure 1. ~~First we applied an automatic algorithm to the raw signal~~
~~of the Polly^{XT} for the detection of the cirrus clouds layers. The method used here is based on a 2. Firstly, the signal to noise~~
 135 ~~ratio (SNR, Eq. 1) is calculated according to the following equation (Georgousis et al., 2015):~~

$$SNR = \frac{C_{sig}}{\sqrt{C_{sig} + C_{bg}}} \quad (1)$$

The SNR is selected above 3.5 (above this threshold value the boundary layers estimation found independent from SNR),
 since the lidar signal is strongly attenuated at higher altitude levels and the noisy parts of the signal should be rejected. Then,
 the zero and background levels are subtracted and the range-corrected signal is calculated. In the next step, we normalize the
 140 ~~range-corrected signal by its maximum value found below 1.5km, so as to enhance the applicability of the method in various~~
~~atmospheric conditions. Given that lidar signals are uncalibrated and signal levels from one lidar system to another can be~~
~~rather different, the normalization ensures the applicability of the criteria used by Baars et al., 2008.~~

After these corrections are made, the Wavelet Covariance Transform (WCT) is applied to the range corrected signal. The
 method used (Eq. ~~1~~), ~~which 2~~, detects discontinuities in the lidar signal, such as the top of the boundary layer, elevated aerosol
 145 layers or cloud boundaries, allowing the detection of cirrus cloud base and top (Brooks, 2003).

$$WCT = \sum_{b-\frac{\alpha}{2}}^b P(z)z^2 dz - \sum_b^{b+\frac{\alpha}{2}} P(z)z^2 dz \quad (2)$$

$$SNR = \frac{C_{sig}}{\sqrt{C_{sig} + C_{bg}}}$$

In Eq. ~~1~~ 2, P(z) is the product profile where the WCT is being applied to. ~~In our case, we apply the wavelet to the range~~
~~corrected signal at 1064nm, after performing the following steps: a) the zero and background levels are subtracted, b) the signal~~

150 is normalized with a maximum value below 1.5km, so as to enhance the applicability of the method in various atmospheric conditions and c) the signal to noise ratio (SNR, Eq. 2) (Georgousis et al., 2015) is above 3.5, since the lidar signal is strongly attenuated at higher altitude levels. It was found that above this threshold the WCT layer estimates were independent from SNR.

155 WCT is the result of the transformation, z is the altitude, β is the height at which a noticeable change in the normalized signal occurs, and α is the dilation chosen. A critical step to the accurate WCT application to the signal is the selection of an appropriate value of the window (dilation), so as to distinguish cloud layers from aerosol layers. In our case, a dilation of 225m, is chosen, proportional to the cirrus geometrical depth (Baars et al., 2008). Another critical step is the threshold WCT value for the determination of the cirrus boundary. A threshold value of 0.1 is selected as a detection limit for both the base (-0.1) and the top (+0.1) of cirrus cloud by (Baars et al., 2008) after sensitivity studies.

160 The WCT transformation has already been applied successfully on cirrus cloud detection (Dionisi et al., 2013). The application of the WCT on a case of cirrus layer observed on July 20th 2016 at Kuopio station, for a time period between 01:00 and 05:00 UTC is presented. In our study, 60-min averages are computed and the respective mean value are taken as cloud base and top height. The mean wavelet applied to the corrected 1064 signal and the particle Depolarization ratio for the whole period of study of the cirrus evolution are presented in Fig. 2.

165 Finally, cloud retrievals from the algorithm are classified as cirrus clouds when the following ~~three~~ four criteria were met: ai) the particle linear depolarization value is higher than 0.25, b) (Chen et al., 2002; Noel et al., 2002), ii) the altitude is higher than 6km and e) iii) the base temperature is below -20-27°C (Goldfarb et al., 2001; Westbrook et al., 2011) and iv) the top temperature is below -38°C (Campbell et al., 2015). The application of these criteria is made so as to avoid ~~water clouds~~ the presence of liquid water. It should be pointed out that lidar measurements were processed only in the absence of lower tropospheric (below 170 4 km) thick clouds.

4 ~~Optical properties of cirrus clouds~~

3.0.1 ~~Retrieval of the optical properties of cirrus~~

175 The application of the WCT on a case of cirrus layer observed on July 20th 2016 at Kuopio station, for a time period between 00:00 and 01:00 UTC is presented. In our study, 60-min averages are computed and the respective mean value are taken as cloud base and top height. The hourly mean wavelet applied to the corrected 1064 signal and the hourly mean particle depolarization ratio and the backscatter coefficient profile of the cirrus evolution are presented in Fig. 3. The temperature values are also plotted with white line and the threshold values are marked with red lines.

3.1 Retrieval of the optical properties of cirrus

The integration of the extinction profile between the defined cloud base and the top of the cirrus layer is calculated to obtain the cirrus optical depth (COD) from the lidar measurements as shown in Eq. (3).

$$COD = \int_{z_{base}}^{z_{top}} a_1(z) dz \quad (3)$$

The night-time measurements from Polly^{XT} were processed by the Raman method, which allows the independent determination of the extinction and backscatter coefficients, thus providing the Lidar-Ratio-lidar ratio (extinction-to-backscatter ratio) (Ansmann et al., 1992). For the retrieval of the cirrus extinction coefficient profiles obtained from the daytime measurements, the integration of the backscatter profile multiplied by the lidar ratio is calculated. The daytime measurements from Polly^{XT} were processed using the Klett inversion (Klett, 1981; Fernald, 1984), with respect to the ratio of the extinction to the backscatter coefficient. These two unknowns have to be related using either empirical or theoretical methods in order to be able to invert the lidar equation. The-In our study, the lidar ratio was determined by comparing the forward and the backward solution of Klett .In our study, and the effective lidar ratio was chosen when value was chosen as the value for which the aforementioned profiles tend to coincide (Ansmann et al., 1992). Both the daytime and night-time optical products were derived for each 1hour averaged profiles. The calculation of the corresponding molecular backscatter and extinction profiles was made based on temperature and pressure profiles obtained from radio soundings. Radiosondes launched daily at 06 and 18 UTC at the Jyvaskyla Airport, located to the southwest (62.39°N, 25.67°E) of the lidar station at Kuopio were used. Radiosonde observations released at Safdarjung Airport (28.58°N, 77.20°E) in New Delhi, India twice a day, and radiosondes from Upington International Airport (28.40°S, 21.25°E), in South Africa were used in the processing of the other two sites. Another important lidar quantity to be calculated is the particle depolarization ratio. This ratio constitutes a qualitative way to discriminate particle shapes and to distinguish spherical from non-spherical particles. Cirrus generally cause enhanced particle depolarization values, higher than 0.25 (see for e.g. Chen et al., 2002), depending on the ice-particle shape and orientation (Lynch et al., 2001). The calibration of the depolarization measurements, needed for the calculation of the particle depolarization ratio, was determined by using the geometric mean of the two $\pm 45^\circ$ measurements, following the procedure described by Freudenthaler et al., (2009). The particle depolarization ratio is presented only for the dataset of Kuopio, as for the other two sites only the Rayleigh calibration method for the calibration measurements was available.

3.1.1 ~~Multiple scattering correction on optical products~~

3.2 Multiple scattering correction on optical products

The lidar equation assumes single scattering from the hydrometeor, but eventually the received photons could have been scattered multiple times before reaching the telescope. This effect, named multiple scattering, is considerably important primarily to the measured extinction coefficient values of cirrus clouds, and secondly to the calculated cirrus optical depth and the esti-

mated ~~Lidar Ratio~~ lidar ratio values. Multiple scattering depends not only on cloud optical depth and cloud extinction, but also on the lidar system components, such as the laser beam divergence and the full-angle field-of-view of the receiver.

210 The relative influence of multiple scattering decreases with increasing height within the cloud, and the errors of the extinction coefficient can be even equal to 60% at the cirrus base (Lynch et al., 2001). ~~Generally~~ As generally, multiple scattering effect cannot be negligible in a receiver field of view equal to 1mrad (Wandinger, 1998). ~~Thus~~, this effect on cirrus clouds optical properties was considered and corrected in this study. In order to calculate the multiple scattering contribution to the calculated optical products, the Eloranta model (Eloranta, 1998) was used to estimate the ratio between the total received power and the

215 contribution of the single scattering, the ratio $P_{tot}(z)/P_1(z) = P_{tot}(z)/P(z)$ (Eq. 4).

~~The effective extinction coefficient aeff~~ The single extinction coefficient a_1 is then related to the actual (~~single~~ multiple scattering) coefficient $a(z)$ through the parameter F as shown in Eq. (5) (Wandinger, 1998). ~~This~~

$$F(\lambda, z) = \frac{\frac{d}{dz} \ln \frac{P_{tot}(z)}{P(z)}}{2a_1(\lambda, z) + \frac{d}{dz} \ln \frac{P_{tot}(z)}{P(z)}} \quad (4)$$

$$a(\lambda, z) = \frac{a_1(\lambda, z)}{1 - F(\lambda, z)} \quad (5)$$

220 The model assumes cirrus ~~made up~~ consist of hexagonal ice crystals and the required inputs are: (i) the laser beam divergence, (ii) the receiver field of view, (iii) the cirrus effective radius, (iv) the measured single scattering extinction profile (or the lidar ratio multiplied by the backscatter for the daytime measurements) and (v) the order of scattering. The estimation of the cirrus effective ~~radii~~ radius was taken from Wang and Sassen (2002), based on the linear relation of the effective radius with the cirrus cloud temperature derived from radio soundings. ~~This~~ For the multiple scattering calculation, the code applies an iterative

225 method including the following steps:

- i) The measured extinction profile of the cirrus layer is provided (a_1).
- ii) With the provided effective radius profile of the cirrus layer (linear relation of the effective radius with the cirrus temperature derived from radio soundings) and the measured extinction coefficient, an iterative procedure provides the ratio $P_{tot}(z)/P(z)$.
- 230 iii) From (ii) a first value for the correcting factor F(z) can be worked out.
- iv) The iterative procedure continues till the calculation of a stable correcting factor F(z) is found.
- v) The corrected extinction can be then calculated from equation (5) and hence the value of lidar ratio.

The model has already been validated against other models (Hogan, 2006) in order to correct the derived optical characteristics of cirrus clouds and has already been applied in cirrus lidar applications (for e.g. Giannakaki et al. 2007). In the following

235 sections, the cirrus optical properties (lidar ratio, extinction coefficient, and optical depth) derived in the frame of this study were corrected for multiple scattering.

$$F(\lambda, z) = \frac{\frac{d}{dz} \ln \frac{P_{tot}(z)}{P_1(z)}}{2a_{eff}(\lambda, z) + \frac{d}{dz} \ln \frac{P_{tot}(z)}{P_1(z)}}$$

$$a_{par}(\lambda, z) = \frac{a^{eff}(\lambda, z)}{1 - F(\lambda, z)}$$

4 Results and discussion

240 In the following section, we present the mean geometrical and optical properties of the detected cirrus layers within the period 2008-2016 ~~from for~~ the three measurement sites, which correspond to subtropical and subarctic regions, and we ~~investigate the expected correlations~~ ~~further discuss the differences~~ between the retrieved properties.

4.0.1 Cirrus cloud cover detection

4.1 Cirrus cloud cover detection

245 Cirrus cloud detection over the three regions is presented in Fig. ~~3-4~~. ~~The detected cirrus clouds over Gual Pahari cannot provide any monthly trend and cannot be representative of an annual pattern. The time periods with technical issues (mentioned above) and the occurrence rate of low clouds observed between March and September led to a limited dataset of cirrus observations. Concerning the annual pattern observed over Elandsfontein, the maximum detection of cirrus layers is reported during May and December. No data processing could be performed during unfavourable weather conditions, such as the presence of low~~
250 ~~cloud, observed mainly the months between January to April with a percentage of ~ 30% of the total measurement period.~~ The analysis of measurements over Kuopio showed that the cirrus cloud cover was found to vary both diurnally and seasonally. From the available data, the ~~frequency-detection~~ of cirrus clouds appears to exhibit an annual pattern with the maximum ~~occurrence from April to October~~ ~~detection from February to September~~ and minimum occurrence during the period between ~~November-October~~ and January, given the favorable meteorological conditions, ~~with no lower clouds~~. Layers of ~~low-water-low~~
255 ~~water~~ clouds were present all year long, with the peak of monthly occurrence between April (28 cases) and November (27 cases). This monthly pattern ~~follows of low clouds existence seems to follow~~ the annual temperature cycle over the region (~~Jylh??, Jylha~~ et al., 2004), with maximum temperature values observed during the period April to October, ~~while November to February are the coldest months~~. Concerning the diurnal pattern, the ~~frequency of number of detected~~ cirrus clouds during ~~night-time nighttime~~ is higher from ~~February to July, and smaller March to Semptember, and lower~~ in the period from ~~August~~
260 ~~October~~ to January.

~~A similar annual pattern of cirrus occurrence frequencies is found over Elandsfontein, but with maximum occurrence during May and December. No data processing could be performed during unfavourable weather conditions, such as the presence of low cloud, observed mainly the months between January to April with a percentage of ~30% of the measurement period.~~

Temperature time-series over the region shows that the cirrus occurrence follows the temperature seasonal cycle, with the minimum values during June-July and the maximum during December (Laakso, et al.)

4.2 Geometrical properties of cirrus clouds over the sub-arctic and tropical sites

Mean cirrus cloud geometrical thickness reported in literature from satellite retrievals is about 2.0 km globally (Sassen et al., 2012). The limited dataset over 2008), while a broad distribution of geometrical boundaries from ground-based systems have been reported in literature (e.g., Gouveia et al., 2017; Seifert et al., 2007; Hoareau et al., 2013). Figure 5 shows the monthly variations of cirrus base height and the cirrus top height (displayed in monthly boxplots) derived with the automated algorithm, with the corresponding mean temperatures above each site. The cirrus geometrical properties show a broad monthly distribution ranging from 6790m to 13070, having the larger variability in the two subtropical sites compared to the subarctic site.

The cirrus lidar dataset in Gual Pahari (given the periods with technical issues) cannot provide any monthly trend and cannot be 28.43°N, 77.15 °E, 243m a.s.l - Northern hemisphere) region is the less extensive one compared to the other two sites and limitations due to the low signal to noise ratios exist. Indeed the sampling might not be statistically representative of the cirrus cloud occurrence. Also, the occurrence rate of low clouds between March and September, minimize the dataset.

4.2.1 Optical and geometrical properties of cirrus clouds over the sub-arctic station of Kuopio (62.74°N, 27.54°E, 190m a.s.l)

Mean cirrus cloud thickness reported in literature is about 2.0 km globally (Sassen properties, but some first results can be discussed. Specifically, during the one-year-long measurement period, Polly^{XT} was measuring on 183 days, corresponding to 2500h in total. The mean value of cirrus base is calculated $9000 \pm 1580\text{m}$, whilst mean top is found to be $10600 \pm 1800\text{m}$, with mean geometrical thickness of $1500 \pm 700\text{m}$. The temperature varied from -27°C to -50°C . Our results are consistent with another study over North China (Min et al., 2008), while lower thickness values from ground-based systems have been reported (e.g., Gouveia et al., 2017). In this study the mean geometrical thickness 2011), based on CALIOP satellite measurements. In this study a value of $1600 \pm 1015\text{m}$ is reported for the cirrus geometrical thickness. According to this study, the cirrus top temperatures were found lower than -50°C and higher than -80°C . A total measurement time of about 4935h corresponding to 88 cirrus profiles have been obtained over Elandsfontein (26.25°S, 29.43°E, 1745m a.s.l - Southern Hemisphere), during the observation period between 11 December 2009 and 31 January 2011, with the exception of the two periods of maintenance of the system (mentioned above). From the cirrus profiles processed, the mean value of cirrus base is calculated to be $1200-9200 \pm 585\text{m}$. Seasonal 810m, while mean top at $10826 \pm 906\text{m}$ for the region of South Africa and the mean geometrical thickness is $1626 \pm 735\text{m}$. For the sub-arctic station of Kuopio (62.74°N, 27.54°E, 190m a.s.l), the seasonal mean cirrus cloud-base heights are calculated as follows: $8725-8363 \pm 1169\text{m}$ (MAM), $8542-8326 \pm 1120\text{m}$ (JJA), $8594-9173 \pm 1100\text{m}$ (SON), and $8300-8900 \pm 1390\text{m}$ (DJF) with an annual mean value of $8597-8600 \pm 1080\text{m}$. The vertical distribution of cloud-base heights shows a broad monthly distribution ranging from 6440m to 11980m. The variability in monthly cirrus cloud base and top heights is shown in Fig-4. The annual mean of the upper boundary of cirrus layers is $9480-9800 \pm 1075\text{m}$, with a maximum value of 12490m during August 12595m during April. The mean geometrical thickness is calculated to be $1200 \pm 700\text{m}$. Base cirrus

temperatures range from -63 – 71°C to -23 – 27°C having a mean value of -40 – 43°C . The corresponding temperature values of the top, range from -71 – 72°C to -31 – 38°C , with a mean value of -48 – 57°C . These values are in accordance with the corresponding ones from the combined data of CloudSat and CALIPSO (Cloud-Aerosol Lidar and Infrared Pathfinder Satellite Observations) measurements (Sassen et al., 2008).

~~In this study, the extinction coefficient at 355nm, averaged over every 1 hour of measurements, ranged from $1.879\text{e-}06$ to $2.7\text{e-}04$, with an annual mean value of $5.47\text{e-}05 \pm 4.3\text{e-}05\text{m}^{-1}$. Seasonal mean extinction values were calculated as: $5.47\text{e-}05$~~
Table 2 summarizes the mean geometrical values calculated for each site separating daytime and nighttime measurements. The averaged geometrical properties between daytime and nighttime are found to be nearly identical above all sites, with differences less than 0.3km.

4.3 Optical properties of cirrus clouds over the sub-arctic and tropical sites

This section presents the cirrus optical properties for the three regions and Figure 6 shows the monthly variations of the cirrus optical properties (displayed in monthly boxplots) above each site.

The COD values over the three sites are presented in Figure 6a and 6b. For the subtropical region of Gual Pahari the mean COD 355 is $0.59 \pm 4.4\text{e-}05$ (MAM), $5.22\text{e-}05$ – 0.25 and the mean COD 532 is found to be $0.45 \pm 3.6\text{e-}05$ (JJA), $5.24\text{e-}05$ – 0.30 . The classification of clouds according to Sassen and Cho (1992), shows that the detected cirrus layers are classified as follows: sub-visible cirrus (0%), optical thin cirrus (20%) and opaque cirrus (80%). One possible reason for the absence of subvisible cirrus clouds in this dataset can be the lower SNR that does not allow detectability of optically thin clouds at Gual Pahari. Another study over North China (Min et al. 2011), reported a mean value of optical depth of $0.41 \pm 3.5\text{e-}05$ (SON), 0.68 at 532nm and the classification of the detected cirrus layers was made as follows: subvisible cirrus (30.26%), optical thin (34.59%) and opaque cirrus (21.54%). Another study over the region (He et al. 2013) reported that the optical depth of the cirrus layers varied between 0.0004 and $7.975\text{e-}05$ – 2.6 , with a mean value of 0.33. For the subtropical region of Elandsfontein the mean value of COD 355 is calculated at $0.35 \pm 7.2\text{e-}05$ (DJF). The corresponding values for the backscatter coefficient range from $1.51\text{e-}07$ to $9.96\text{e-}06$ with an annual value of $1.769\text{e-}06$.

Column-integrated 0.03 and the mean COD 532 is found to be 0.30 ± 0.30 . The COD have their highest values between April (1.36) and May (1.33) and December (1.02) and the percentage of 2% is categorized as subvisible cirrus, 61% as thin cirrus and 37% as opaque cirrus. For the Kuopio, the column-integrated mean corrected COD at 355nm is 0.25 ± 0.2 , and is found to vary between 0.018 and 1.53, while the mean COD 532 is found to be 0.231 – 0.24 ± 0.18 – 0.20 . The highest values of AOD-COD are found between January and March. To further investigate the distribution of the cirrus optical depth, we present a histogram of cirrus cloud optical depth in Fig. 5a and Fig. 5b. The most predominant values of cirrus optical depth are between 0.1 and 0.4, with the highest value of 0.95. The mean COD 355 calculated in this study is larger than the value of 0.16 ± 0.27 reported by Das et al. (2009) and smaller than the value of 0.41 ± 0.68 reported by Min et al. (2011) from mid-latitude observations. And at the same time, a number of studies midlatitude observations. A number of other studies have reported mean COD values between 0.2 and 0.4. The mean cirrus optical depth reported for a tropical region is 0.25 ± 0.46 (Gouveia et al., 2017), for example, while the overall mean value of cirrus optical depth for a midlatitude station found to be

0.37 ± 0.18 (Dionisi et al., 2013). Reichardt (1998) reported that cirrus clouds optical depth values were lower than 0.3 for 70% of the cases processed for northern midlatitude cirrus. The classification of cirrus clouds according to Sassen and Cho (1992) indicates that 3.13% of the cirrus clouds measured in Kuopio are subvisible ($\tau < 0.03$), 70.71% are thin cirrus ($0.03 < \tau < 0.3$) and 26.926% are opaque cirrus ($\tau > 0.3$). The low percentage of the subvisible category of cirrus layers, have also been
335 observed over midlatitude sites (e.g., ~~Kienast-Sjogren~~ Kienast-Sjogren et al., 2016), where subvisible cirrus clouds have been measured during 6% of the observation time.

In what follows we proceed into finding a connection between the COD values derived in the different sites and the AOD load over the regions which are exposed to different aerosol sources. Table 4 lists the predominant aerosol type over each region and the results from the analysis of AOD at 355 nm in the free troposphere and the calculated COD values. We can conclude
340 that there is an indication of the relationship of the aerosol load on the derived cirrus statistics, as the higher AOD values are linked with the higher COD values calculated for the two subtropic regions. More specifically, the one year aerosol analysis of lidar observations in Gual Pahari (Komppula et al., 2012) showed that in the summer, the measured air masses were slightly more polluted and the particles were a bit larger than in other seasons (higher Angstrom exponent values), with the main aerosol sources to be the local and regional biomass and fossil fuel burning. The annual averages revealed a distinct seasonal pattern
345 of aerosol profiles, with aerosol concentrations slightly higher in summer (June - August) compared to other seasons, and particles larger in size. During the summer and autumn, the average lidar ratios were larger than 50 sr, suggesting the presence of absorbing aerosols from biomass burning. The lidar observations that were performed at Elandsfontein and used for aerosol characterization for the corresponding study period (Giannakaki et al. 2016) showed that the observed layers were classified as urban / industrial, biomass burning, and mixed aerosols using the information of backward trajectories, MODIS hotspot
350 fire products and in situ aerosol observations. The analysis of the seasonal pattern of vertical profiles of the aerosol optical properties showed that the more absorbing (higher lidar ratio at 355 nm) biomass particles were larger on August and October, while the category of Urban/industrial had their peak on January, March and May. Kuopio is an urban area and constitutes a low aerosol content environment. The columnar analysis of sunphotometer observations (Aaltonen et al., 2010) revealed that the high Angstrom exponent values observed can be possible linked with the presence of fine particles, while the seasonal
355 analysis of the optical depth showed that there is no significant variation.

Concerning the lidar ratios values (Figure 6c and 6d) observed over Gual Pahari, the lidar ratio value at 355nm is calculated at 27 ± 12 sr and the corresponding one for 532nm is 28 ± 22 sr and the lidar ratios reach their highest values on May. Our results are in agreement with another cirrus cloud study for the area; He et al. (2013) report a mean lidar ratio value of 28 sr, using a micropulse lidar. For the Elandsfontein site, the mean LR 355 value is found to be 26 ± 6 sr and the mean LR 532
360 is 25 ± 6 sr and the lidar ratios reach their highest values during April. A mean value Lidar Ratio-lidar ratio of 33 ± 7 sr at 355nm is observed for the whole period studied, with a variability of less than 1.5 sr for the different seasons (Fig. 6) over Kuopio site, with higher variability observed on June, while the corresponding mean value LR 532 is calculated to be 30.4 ± 3.1
 ± 7.5 sr, without any obvious seasonal cycle. Specifically, the mean LR 355 for the corresponding months are calculated as follows: 33 ± 7 sr (MAA), 33.2 ± 7.3 sr (JJA), 32.9 ± 7 sr (SON) and 32.3 ± 5 sr (DJF). For opaque, thin and sub-visible
365 cirrus clouds the means are 30.3 ± 6 sr, 33.8 ± 7.1 sr, and 34.4 ± 7.4 sr, respectively. Gouveia et al. (2017) found

a mean LR 355 value of 23.9 ± 8.0 sr (SD) for the tropical region of Amazonia, while Giannakaki et al., (2007), reported a corresponding value of 30 ± 17 sr for a mid-latitude station. Josset et al. (2012) and Garnier et al. (2015) analyzed spaceborne CALIOP (Cloud Aerosol Lidar with Orthogonal Polarization) lidar observations. Both studies concluded that cirrus lidar ratio (corrected for multiple scattering effects) around the globe has typically values of ~~30-35sr~~ $30-35$ sr \pm ~~5-8sr~~ $5-8$ sr at 532 nm. Nevertheless, the lidar ratio values may vary greatly depending not only on the altitude and composition of the cirrus clouds (Goldfarb et al., 2001), but also on the correction of the multiple scattering effect (Platt, 1981; Hogan, 2008). The aforementioned depends on the ice crystals effective radius and the associated uncertainty could range from 20 to 60% (Wandinger, 1998). Lidar ratio for cirrus clouds ~~is was~~ assumed to be constant with altitude and season with a value of 25 sr using the CALIOP extinction retrieval algorithm (Young et al., 2013; Young and Vaughan, 2009), but this value has changed in the upgraded algorithm, as illustrated by Young et al. (2018).

Concerning the monthly variability of the depolarization values (Figure 6e) over Kuopio, no clear tendency is observed. The higher monthly mean value was observed on July, but the variability was less than 0.04 between months, with a mean value of 0.38 ± 0.07 . ~~Fig. 5c and Fig. 5d presents the histograms of the lidar ratio corrected for multiple scattering, with the~~

As the assumption that the backscatter and the extinction coefficients for sufficiently large cirrus particles are spectrally independent; the color ratio (ratio of backscatter profiles, CR) at 355 and 532 is supposed to be equal one. This assumption is also used in satellite processing schemes. However, it is reported that the measured variability of cirrus color ratios is much larger than previously realized and that measured color ratios are higher in the tropics (Vaughan et al., 2010). For the Kuopio station, mean CR is found 1.1 ± 0.8 , while for the less extensive dataset of New Delhi the mean value is found 1.5 ± 0.8 and for Elandsfontein the mean value is 1.4 ± 1.1 .

Table 3 summarizes the mean optical values discussed above, for the three sites, separating daytime and nighttime observations. Generally, the averaged optical properties values are found to be nearly identical, except one site (New Delhi), where average nighttime optical properties found higher (~ 4 sr) than that of daytime.

To further investigate the distribution of the cirrus lidar ratio values over Kuopio, we present a histogram of the values derived in Fig. 7. The most frequent observed lidar ratio values ranging between 28 and 36 sr for 355 nm and 20 and 36 sr for 532 nm. Similar results have been retrieved regarding the variability of LR 532, which is constant from one month to another (~~not shown here~~), as shown. This figure can provide an evidence that although the lidar dataset are not continuous (due to not favour weather conditions the winter months), the frequency distributions are close to normal and thus the statistics shown here have a significance. In addition we can claim that with this scarce sample of data we observe consistent results with a number of other literature studies.

In Figure 78, we examine the dependence of the LR 355 with the COD 355 values on intervals of 5 sr. The dashed lines indicate the categories defined by Sassen and Cho (1992). The most common lidar ratio values from 25 to 40 sr are found for the lowest COD values. Furthermore, the dependence of the lidar ratios at 355nm with the cirrus cloud base temperature is also examined. No dependence of the lidar ratio with cloud base temperature is found, indicating that cirrus are vertically well mixed (Liu et al., 2015).

400 **4.3.1 Optical and geometrical properties of cirrus clouds over the sub-tropical region of Gual Pahari (28.43°N, 77.15**
°E, 243m a.s.l) ??? Northern hemisphere

The cirrus lidar dataset in this region is the less extensive one compared to the other two sites and limitations due to the low signal to noise ratios exist. Indeed the sampling might not be statistically representative of the cirrus cloud properties, but some first results can be discussed. Specifically, during the one year long measurement period, Polly^{XT} was measuring on 183 days, corresponding to 2500h in total. The mean value of cirrus base is calculated $8947 \pm 1465\text{m}$, whilst mean top is found to be $10235 \pm 1500\text{m}$, with mean geometrical thickness of $1295 \pm 489\text{m}$. The temperature varied from -20°C to -50°C . The mean COD 355 is 0.59 ± 0.39 and the mean COD 532 is found to be 0.43 ± 0.37 . The Lidar Ratio value at 355nm is calculated at $25.6 \pm 12\text{ sr}$ and the corresponding one for 532nm is $27 \pm 16\text{ sr}$. The AOD have their highest values between May and August and the lidar ratios reach their highest values in May. The cirrus layers detected are mostly classified as opaque layers (68%).

405

410 Our results agree with another cirrus cloud study for the area; He et al. (2012) report a mean lidar ratio value of 28 sr, using a micropulse lidar. According to their study, the optical depth of the cirrus layers varied between 0.0004 and 2.6, with mean value of 0.33. The detected cirrus clouds were classified as follows: sub-visible cirrus (0%), optical thin cirrus quite low COD values (27%) and opaque cirrus (72%). One possible reason for the occurrence frequency of subvisible cirrus clouds in this dataset can be the lower SNR that does not allow detectability of optically thin clouds at Gual Pahari. Another study over North China

415 (Min et al., 2011), based on CALIOP satellite measurements, reported a value of $1600 \pm 1015\text{m}$ for the cirrus geometrical thickness. According to their study, the cirrus top temperatures were found lower than -50°C and higher than -80°C . Concerning the optical properties, a mean value of optical depth of 0.41 ± 0.68 at 532nm was reported. The detected cirrus layers were classified as follows: subvisible cirrus (30.26%), optical thin (34.59%) and opaque cirrus (21.54%) corresponding to thin cirrus) for the subarctic station.

420 **4.3.1 Optical and geometrical properties of cirrus clouds over the sub-tropical region of Elandsfontein (26.25°S,**
29.43°E, 1745m a.s.l) ??? Southern Hemisphere

A total measurement time of about 4935h corresponding to 88 cirrus profiles have been obtained over Elandsfontein, during the observation period between 11 December 2009 and 31 January 2011, with the exception of the two periods of maintenance of the system (mentioned above). From the cirrus profiles processed, the mean value of cirrus base is calculated to be $8477 \pm 858\text{m}$, while mean top at $10015 \pm 906\text{m}$ for the region of South Africa and the mean geometrical thickness is $1383 \pm 735\text{m}$. The mean value of COD 355 is calculated at 0.4 ± 0.3 and the mean COD 532 is found to be 0.324 ± 0.319 . The AOD have their highest values in the autumn and the lidar ratios reach their highest values in the autumn and winter. A percentage of 4% is categorized as subvisible cirrus, 52% as thin cirrus and 44% as opaque cirrus. The mean LR 355 value is found to be $25 \pm 6\text{ sr}$ and the mean LR 532 is $24 \pm 6\text{ sr}$. As a limited number of long-term cirrus measurements are carried out in the Southern

425

430 Hemisphere and only information from satellite observations have been published, especially for the geometrical properties (Sassen et al., 2008), no comparison with previous studies can be conducted for the region and the information reported here, to our knowledge, represents the longest ground-based lidar dataset of cirrus properties.

4.3.1 Cirrus classification

4.4 Cirrus classification at Kuopio

435 The classification of cirrus clouds according to Sassen and Cho (1992) is made based on the COD values. Ground-based lidars are well suited for thin cirrus layers observations, due to their sensitivity to thin atmospheric features, in contrast to spaceborne lidar observations (Martins et., 2011). For this reason, additional analysis on each cirrus category is also ~~Conducted for Kuopio~~ conducted for Kuopio site as measurements in this station represent the most extensive dataset ~~with a set of 224 cirrus cases acquired~~ between November 2012 and December 2016.

440

Category "Subvisible"

Subvisible cirrus are geometrical thin layers with mean geometrical thickness of 643 ± 211 m. Generally, subvisible cirrus detection is a challenging component in satellite retrievals. MODIS, for example, is not sensitive to optically thin cirrus clouds due to the insufficient contrast with the surface radiance (Ackerman et al., 2008; Ackerman et al., 2010), while the CALIPSO and CloudSat observations are more sensitive to the height and presence of subvisible and thin cirrus (Hong et al., 2010). Thus, the mapping of subvisible cirrus can be rather important in climatological studies. In our study, 6 cases of cirrus with COD less than 0.03 are analyzed, mostly detected during February. Subvisible cirrus geometrical thickness found 750 ± 269 m, less than the mean value of all cirrus clouds, and their temperature ~~2??C-3???~~ $2^{\circ}\text{C}-3^{\circ}\text{C}$ colder than the mean temperature. These values are consistent with previous studies of subvisible cirrus from spaceborne lidar observations, examined on a global scale (Martins et., 2011). Their mean COD 355 is calculated 0.021 ± 0.0031 , their mean LR 355 ~~was is~~ 34 ± 7 sr and their mean particle depolarization value is 0.45.

450

Category "Thin"

As mentioned previously, thin cirrus is the most predominant type of cirrus in our study, with ~~161~~ 152 observations. Thin cirrus can also be undetectable by passive remote-sensing satellites, especially the ones with COD less than 0.2, and have so far not systematically been characterized. Their geometrical thickness found to be 1100 ± 586 m. Their mean COD 355 is calculated 0.16 ± 0.07 , their mean LR 355 is 34 ± 7 sr and their mean particle depolarization value is 0.3 ± 0.13 .

455

Category "Opaque"

460 Opaque cirrus are the one with the highest value of optical depth that contribute the most of the total radiative forcing (~~Kienast-Sj??gren~~ Kienast-Sjogren et al., 2016). In our study, a total of ~~62~~ 55 measurements of opaque cirrus are processed. Their mean geometrical thickness is found to be 1462 ± 659 m, higher than the value of all cirrus categories. Their mean COD 355 is calculated 0.5 ± 0.21 , their mean LR 355 ~~was is~~ 31 ± 6 sr and their mean particle depolarization value is 0.33 ± 0.12 .

4.4.1 ~~Temperature and latitudinal dependence of cirrus properties~~

465 4.5 Latitudinal and temperature dependence of cirrus properties

The three presented datasets are derived from different latitudinal and climatic sites. In this section we ~~examine the lidar products profile shape and the~~ firstly examine the latitudinal dependence of the cirrus geometrical and optical properties ~~on cirrus base temperature. The mean and standard deviation of the Lidar Ratio and percentages of each cirrus class. The reported values in literature from previous studies based on lidar groundbased dataset and the retrievals of the current one~~ are listed in Table ~~2-5~~ and plotted in Figure 9 for comparison. We can note, that the cirrus geometrical properties and the lidar ratio values may vary greatly depending on the latitude and an decreasing trend of the geometrical boundaries with the rise of the distance from the equator is obvious, also reported by satellite observations (Sassen et al., 2008). Generally, cirrus layers have been observed up to altitudes of 13km above ~~Gual Pahar~~ the subtropical sites, whereas they have only been detected to about 1km lower at the ~~other two regions~~ subarctic region and this conclusion is in accordance with the Cloudsat observations (Sassen et al., 2008). Based on the satellite information, the derived cirrus cloud thicknesses ~~were was~~ found to be larger in the tropics and decreasing toward the poles. Also, ~~larger values of COD-355 and smaller LR were from the values reported from groundbased studies, a pattern can be concluded: cirrus cloud geometrical properties peaks around the equator and at midlatitudes sites, with generally decreasing amounts as the poles are approached. On the other hand, the lidar ratio values seem to follow a diverse relation, showing greater values moving to the poles. In our study, lower LR are~~ observed for Gual Pahari and Elandsfontein and higher mean value for Kuopio. The larger variability of the optical properties at the two subtropical regions, relative to Kuopio, could be related to the larger and variable aerosol load over these regions. Overall, our results seem to demonstrate that subarctic cirrus clouds are colder, lower and optical thinner than subtropical cirrus clouds. However, a more extended database is needed to strengthen these indications.

The dependence of geometrical and optical properties on ~~cirrus base~~ mid-cirrus temperature is also examined in Fig. ~~8. The number of cases per temperature bin are also labeled. 10.~~ In order to investigate this dependence, we have grouped cirrus clouds temperatures into 5°C intervals. The number of cases per temperature bin are also labeled. Temperature values are obtained from radio soundings, as mentioned above. Thicker clouds (~ 1.5 km) are observed at temperatures between ~ -40 to -45°C and $\sim -35^\circ\text{C}$, decreasing in thickness with decreasing thickness reported for lower temperatures, for both the subtropic and subarctic regions. ~~This trend is also~~ and a second peak is found in the range between $\sim -75^\circ\text{C}$ and $\sim -65^\circ\text{C}$ for the subarctic station. A similar trend has been reported for a midlatitude region by Hoareau et al. (2013), where thickest cirrus layers were found about -42.5°C , and thinner ones at both colder and warmer temperatures. Another study (Pandit et al., 2015) reports that the geometrical thickness increases from 1 to 3.5 km as mid-cloud temperature increases from -90 to -60°C , while for the further increase in temperature from -60 to -20°C , the geometrical thickness decreases to less than 1 km. Concerning the optical properties shown in Fig. 10, ~~there~~ a steady increase of lidar ratio from -25°C to -40°C is noticed for the two subtropical stations, while the variability of this parameter is relatively constant across months for the subtropic station, with a slightly increase at warmer temperatures (Figure 10b). There are indications that the cloud optical depth increases with the increasing cirrus ~~temperature base~~ mid temperature for the two subtropical sites (Fig. 10c). At cold temperatures ($\sim -65^\circ\text{C}$),

optical thickness for cirrus layers of the subarctic station is high, compared to warmer temperatures and also cloud thickness for this temperature is similar high (~ 1.5 km). The dependence of the ~~lidar ratio and the~~ particle depolarization values on base temperature is also examined (Fig. ~~10b and Fig.~~ 10d). No clear tendency is found ~~for the lidar ratio~~, as the variability of this parameter is relatively constant ~~across months for both subarctic and subtropic regions, while,~~ with a slightly increase of the particle depolarization ~~increases with the decreasing temperature~~ base with the increasing mid temperature. This behaviour indicates a relation between cirrus ice crystal shape and temperature ~~and has been also reported for a midlatitude station (Sassen et al., 2001).~~ ~~However,~~ however, more studies should be done in order to examine this behaviour on various geographical locations.

Figure 11 presents the color ratios values on 5°C intervals of cirrus mid temperature, indicating an almost stable behavior with temperature. Generally, we can conclude that for higher altitudes, lower spectral dependence is noticed, taking also into account the number of measurements performed at each site.

The dependency of the mid temperature with the lidar ratio values at 355nm and the particle depolarization values is further examined (Figure 12). Fig. 12 shows that the highest values of cirrus lidar ratio (>40) correspond to higher values of cirrus depolarization (>0.4) and warmer cirrus. Moreover, it can be seen the variety of depol values that correspond to the mean value of lidar ratio (~ 31). A similar behavior is reported in Chen et al. (2002) for lidar ratio values higher than 30 sr. In his study, the relationship between the depolarization ratio and the lidar ratios shows the former split into two groups for lidar ratios higher than 30. The first group has high depolarization ratios about 0.5 and the second one has 0.2.

515 5 Conclusions

Observations of cirrus clouds geometrical and optical properties, performed with a ground-based multi-wavelength Polly^{XT} Raman Lidar, during the period 2008 to 2016 are analyzed and presented in this study. The measurements were performed in three places at different latitudes, Gual Pahari (28.43°N, 77.15°E, 243m a.s.l) in India, Elandsfontein (26.25°S, 29.43°E, 1745m a.s.l) in South Africa and Kuopio (62.74 °N, 27.54°E, 190m a.s.l) in Finland. ~~An and an~~ algorithm is developed to automatically define the cirrus clouds boundaries. ~~The vertical profiles of the backscatter, extinction, and lidar ratio and the monthly patterns of the geometrical characteristics and optical properties of cirrus layers are presented.~~

~~Our results show that cirrus layers having a noticeable month-to-month variation, with slightly higher geometrical values in summer compared to other seasons for the subtropical northern hemisphere.~~ The statistical behaviour of the cirrus clouds properties in the different geographical and climatic counterparts shows that the geometrical boundaries display large distribution for the two subtropical regions with higher values of geometrical thickness, with mean thickness of ~~1295-1500 ± 489m, 1383-700m, 1600 ± 735m and 1200 ± 585m-700m~~ for Gual Pahari, Elandsfontein and Kuopio respectively, showing their dependence on the geographical location. The corresponding overall mean value of COD 355 is calculated to be ~~0.59-0.60 ± 0.39 and 0.40-0.25 and 0.35 ± 0.33, 0.30~~, for Gual Pahari and Elandsfontein correspondingly, while a slightly lower mean of 0.25 ± 0.2 is calculated for Kuopio. The lidar ratio values at 355nm ~~are found to be 26~~ show higher values moving to the poles, with calculated values to be 27 ± 12 sr, ~~25-26 ± 6 sr, and 33 ± 7 sr~~ for Gual Pahari, Elandsfontein and Kuopio, respectively.

~~Generally the optical properties have their highest values in the subtropical region of the northern hemisphere.~~ Overall, our results seem to demonstrate that subarctic cirrus clouds are colder, lower, and optical thinner than subtropical cirrus clouds. However, a more extended database is needed to strengthen these indications.

The dependence of cirrus clouds geometrical thickness and optical properties on base-mean temperature is also examined, showing quite similar tendency, but less variability for the subarctic dataset. The dependence of cirrus clouds geometrical thickness and optical properties on mid temperature shows quite similar tendency, but less variability for the subarctic dataset. Cirrus found geometrical ~~thickest (geometrically and optically) at temperatures -40~~ and optical thickest at temperatures between -45°C and -35°C. At temperatures ~~of -65~~ below -55°C, the optical thickness of cirrus layers ~~is high, compared to warmer temperatures and also cloud thickness for this temperature is similar high (~1.5 km)~~ becomes again high and this trend appears only for the subarctic station. ~~The lidar ratio~~ However, we should keep in mind that the number of samples corresponding to temperatures below -60°C is limited. The lidar ratio is found to be quite constant with temperature, with a slightly increase in the warmer mid temperatures, showing larger variability for the subtropic datasets, while the particle depolarization values ~~increases with the decreasing temperature base~~ seem almost constant at temperatures between -27°C and -60°C.

The geometrical and optical properties of cirrus layers are studied in detail, providing information useful in the validation of the cirrus parameterizations in models. Furthermore, our results could be useful for lidar ratio selection schemes needed by satellite optical properties retrievals of cirrus layers over different locations, e.g., the upcoming EarthCARE (Earth Cloud Aerosol and Radiation Explorer) mission. The spectral dependence discussed above, is another important issue for the satellite algorithm schemes, given the different wavelengths applied among the different satellites.

In any case, further cirrus observations must be conducted, so as to ~~investigate whether~~ investigate whether differences in the background aerosol load contribute to potential differences in the cirrus cloud geometrical and optical properties and which are the different atmospheric mechanisms leading to these differences over the different regions.

Author contributions. KA. Voudouri prepared the automatic algorithm for the cirrus detection and processed the lidar measurements for the optical retrievals during the period 2008-2016. KA. Voudouri prepared the figures of the manuscript. E. Giannakaki reviewed parts of the results. M. Komppula is the PI of the lidar station and D. Balis directed the preparation of the manuscript. KA. Voudouri prepared the manuscript with contributions from all co-authors.

Competing interests. The authors declare that they have no conflict of interest.

Acknowledgements. This work has been conducted in the framework of EARLINET (EVR1 CT1999-40003), EARLINET ASOS (RICA-025991), ACTRIS, and ACTRIS-2 funded by the European Commission. The research leading to these results has received funding from the European ~~Union?~~ Union's Horizon 2020 research and innovation program under grant agreement no. 654109 and previously from the European Union Seventh Framework Programme (FP7/~~2007???~~ 2013-2013) under grant agreement no. 262254. This work was partly

funded by the European Commission 6th Framework under the European Integrated Project on Aerosol Cloud Climate and Air Quality Interactions, EUCAARI. Voudouri K.A acknowledges the support of the General Secretariat for Research and Technology (GSRT) and Hellenic Foundation for Research and Innovation (HFRI). (Scholarship Code: 95041).

References

- 565 [Aaltonen, Veijo & Rodriguez, Edith & Kazadzis, Stelios & Sogacheva, Larisa & Arola, Antti & de Leeuw, Gerrit.: Characteristics of the aerosol climatology over Finland based on the optical columnar properties. 12. 10788, 2010.](#)
- Ackerman, S., Holz, R., Frey, R., and Eloranta, E.: Cloud Detection with MODIS: Part II Validation, *J. Atmos. Ocean. Tech.*, 25, [1073-1086](#), doi:10.1175/2007JTECHA1053.1, 2008.
- Ackerman, S., Frey, R., Strabala, K., Liu, Y., Gumley, L., Baum, B., and Menzel, P.: Discriminating Clear-Sky From Cloud With MODIS, Algorithm Theoretical Basis Document (MOD35), ATBD Version 6.1, 2010.
- 570 Althausen D., Engelmann R., Baars H., Heese B., Ansmann A., Muller D., Komppula M.: Portable Raman lidar Polly^{XT} for automated profiling of aerosol backscatter, extinction, and depolarization. *J. Atmos. Ocean. Tech* 26:2366-2378. Doi10.1175/2009JTECHA1304.1, 2009.
- Ansmann, A., Wandinger, U., Riebesell, M., Weitkamp, C., and Michaelis, W.: Independent measurement of extinction and backscatter profiles in cirrus clouds by using a combined Raman elastic-backscatter lidar, *Appl. Opt.*, 31, [7113-7131](#), 1992.
- 575 Baars, H., Ansmann, A., Engelmann, R., and Althausen, D.: Continuous monitoring of the boundary-layer top with lidar, *Atmos. Chem. Phys.*, 8, 7281-7296, <https://doi.org/10.5194/acp-8-7281-2008>, 2008.
- Beyerle G., Gross M. R., Haner D. A., Kjome N. T., McDerimid I. S., McGee T. J., Rosen J. M., Schafer H. J., and Schrems O.: A lidar and backscatter sonde measurement campaign at Table Mountain during [February-March](#) 1997: observations of cirrus clouds, *J. Atmos. Sci.* 58, [1275-1287](#), 2001.
- 580 Brooks, I.: Finding Boundary Layer Top: Application of a wavelet covariance transform to lidar backscatter profiles, *J. Atmos. Ocean. Tech.*, 20, [1092-1105](#), 2003.
- Campbell, J. R., Vaughan, M. A., Oo, M., Holz, R. E., Lewis, J. R., and Welton, E. J.: [Distinguishing cirrus cloud presence in autonomous lidar measurements, Atmos. Meas. Tech.](#), 8, 435-449, doi:10.5194/amt-8-435-2015, 2015.
- 585 [Campbell, J., Lolli, S., Lewis, J., Gu, Y., and Welton, E.: Daytime Cirrus Cloud Top-of-the-Atmosphere Radiative Forcing Properties at a Midlatitude Site and Their Global Consequences, J., Appl. Meteorol. Clim.](#), 55, [1667-1679](#), doi:10.1175/JAMC-D-15-0217.1, 2016.
- Chen, Wei-Nai & Chiang, Chih-Wei & Nee, Jan.: Lidar Ratio and Depolarization Ratio for Cirrus Clouds. *Applied optics*. 41. 6470-6. 10.1364/AO.41.006470, 2002.
- 590 Comstock, J. M., Ackerman, T. P., and Mace, G. G.: Ground-based lidar and radar remote sensing of tropical cirrus clouds at Nauru Island: Cloud Statistics and radiative impacts, *J. Geophys. Res.*, 107, 4714, doi:10.1029/2002JD002203, 2002.
- Das, S.K., Nee, J.B., Chiang, C.W.: A LiDAR study of the effective size of cirrus ice crystals over Chung-Li, Taiwan. *J. Atmos. Terr. Phys.* 72 (9-10), [781-788](#). <http://dx.doi.org/10.1016/j.jastp.2010.03.024>, 2010.
- Dionisi D., Keckhut P., Liberti G. L., Cardillo F., and Congeduti F.: Midlatitude cirrus classification at Rome Tor Vergata through a multichannel [Raman-Mie-Rayleigh](#) lidar, *Atmos. Chem. Phys.*, 13, [11853-11868](#), www.atmos-chem-phys.net/13/11853/2013/doi:10.5194/acp-13-11853-2013, 2013.
- [Dupont, J.-C., M. Haeffelin, Y. Morille, V. Noel, P. Keckhut, D. Winker, J. Comstock, P. Chervet, and A. Roblin, Macrophysical and optical properties of midlatitude cirrus clouds from four ground-based lidars and collocated CALIOP observations, J. Geophys. Res.](#), 115, D00H24, doi:10.1029/2009JD011943, 2010.

- 600 Eloranta, E.: Practical model for the calculation of multiply scattered lidar returns, *Appl. Opt.*, 37, [2464-2472](#), doi:10.1364/ao.37.002464, 1998.
- Engelmann, R., Kanitz, T., Baars, H., Heese, B., Althausen, D., Skupin, A., Wandinger, U., Komppula, M., Stachlewska, I.S., Amiridis, V., Marinou, E., Mattis, I., [Linné, H.](#), and Ansmann, A.: The automated multiwavelength Raman polarization and water-vapor lidar Polly^{XT}: the neXT generation, *Atmos. Meas. Tech.*, 9, 1767-1784, <https://doi.org/10.5194/amt-9-1767-2016>, 2016.
- 605 Engelmann R., Kanitz T., Baars H., Heese B., Althausen D., Skupin A., Wandinger U., Komppula M., Stachlewska IS, Amiridis V., Marinou E., Mattis I., Linné H., Ansmann A.: EARLINET Raman lidar Polly^{XT}: the next generation. *Atmos Meas Tech Discuss* 8:7737-7780. doi10.5194/amtd-8-7737-2015, 2015.
- Fernald, F.G.: Analysis of atmospheric lidar observations, some comments, *Applied Optics*, vol. 32, pp. 652-653, 1984.
- Filioglou, M., Nikandrova, A., [Niemelä, S.](#), Baars, H., Mielonen, T., Leskinen, A., Brus, D., Romakkaniemi, S., Giannakaki, E., and Komppula, M.: Profiling water vapor mixing ratios in Finland by means of a Raman lidar, a satellite and a model, *Atmos. Meas. Tech.*, 10, 4303-4316, <https://doi.org/10.5194/amt-10-4303-2017>, 2017.
- 610 Freudenthaler, V., Esselborn, M., Wiegner, M., Heese, B., Tesche, M., Ansmann, A., Müller, D., Althausen, D., Wirth, M., Andreas, F. I. X., Ehret, G., Knippertz, P., Toledano, C., Gasteiger, J., Garhammer, M., and Seefeldner, M.: Depolarization ratio profiling at several wavelengths in pure saharan dust during SAMUM 2006, *Tellus B*, 61, [165-179](#), 2009.
- 615 Garnier, A., Pelon, J., Vaughan, M. A., Winker, D. M., Trepte, C.R., and Dubuisson, P.: Lidar multiple scattering factors inferred from CALIPSO lidar and IIR retrievals of semi-transparent cirrus cloud optical depths over oceans, *Atmos. Meas. Tech.*, 8, [2759-2774](#), doi:10.5194/amt-8-2759-2015, 2015.
- Giannakaki, E., van Zyl, P. G., [Müller, D.](#), Balis, D., and Komppula, M.: Optical and microphysical characterization of aerosol layers over South Africa by means of multi-wavelength depolarization and Raman lidar measurements, *Atmos. Chem. Phys.*, 16, 8109-8123, <https://doi.org/10.5194/acp-16-8109-2016>, 2016.
- 620 Giannakaki, E., [Pfleger, A.](#), [Korhonen, K.](#), [Mielonen, T.](#), [Laakso, L.](#), [Vakkari, V.](#), [Baars, H.](#), [Engelmann, R.](#), [Beukes, J. P.](#), [Van Zyl, P. G.](#), [Josipovic, M.](#), [Tiitta, P.](#), [Chiloane, K.](#), [Piketh, S.](#), [Lihavainen, H.](#), [Lehtinen, K. E. J.](#), and [Komppula, M.](#): One year of Raman lidar observations of free-tropospheric aerosol layers over South Africa, *Atmos. Chem. Phys.*, 15, 5429-5442, <https://doi.org/10.5194/acp-15-5429-2015>, 2015.
- 625 [Giannakaki, E.](#), Balis, D. S., Amiridis, V., and Kazadzis, S.: Optical and geometrical characteristics of cirrus clouds over a Southern European lidar station, *Atmos. Chem. Phys.*, 7, [5519-5530](#), doi:10.5194/acp-7-5519-2007, 2007.
- Georgousis G., Adam M., and Avdikos G.: Signal to noise ratio estimations for a volcanic ash detection lidar. Case Study: Met Office, 27 th International Laser Radar Conference: 5-10 July, New York, USA, 2015.
- Gouveia Diego A., Barja B., Barbosa H. M. J., Seifert P., Baars H., Pauliquevis T., and Artaxo P.: Optical and geometrical properties of cirrus clouds in Amazonia derived from 1 year of ground-based lidar measurements, *Atmos. Chem. Phys.*, 17, [3619-3636](#), www.atmos-chem-phys.net/17/3619/2017/, doi:10.5194/acp-17-3619-2017, 2017.
- 630 He, Q. S., and Coauthors: The properties and formation of cirrus clouds over the Tibetan Plateau based on summertime lidar measurements. *J. Atmos. Sci.*, 70, [901-915](#), doi:<https://doi.org/10.1175/JAS-D-12-0171.1>, 2013.
- Hoareau, Christophe & Keckhut, Philippe & Noel, Vincent & Chepfer, H & Baray, J.: A decadal cirrus clouds climatology from ground-based and spaceborne lidars above the south of France (43.9°[N-5.7°E](#)). *Atmospheric Chemistry and Physics*. 13. 10.5194/acp-13-6951-2013, 2013.
- 635

- Hogan, R. J. and Kew, S. F.: A 3D stochastic cloud model for investigating the radiative properties of inhomogeneous cirrus clouds, *Q. J. Roy. Meteor. Soc.*, 131, [2585-2608](#), 2005. Hogan, R. J.: "Fast approximate calculation of multiply scattered lidar returns," *Appl. Opt.* 45, 5984-5992, 2006.
- 640 Hong, G., Yang, P., Heidinger, A. K., Pavolonis, M. J., Baum, B. A., and Platnick, S. E: Detecting opaque and nonopaque tropical upper tropospheric ice clouds: A trispectral technique based on the MODIS 8-12 μm window bands, *J. Geophys. Res.*, 115, D20214, doi:10.1029/2010JD014004, 2010.
- Illingworth, A. J., R. J. Hogan, E. J. O'Connor, D. Bouniol, M. E. Brooks, J. Delanoë, D. P. Donovan, J. D. Eastment, N. Gaussiat, J. W. F. Goddard, M. Haeffelin, H. Klein Baltink, O. A. Krasnov, J. Pelon, J.-M. Piriou, A. Protat, H. W. J. Russchenberg, A. Seifert, A. M. Tompkins, G.-J. van Zadelhoff, F. Vinit, U. Willen, D. R. Wilson and C. L. Wrench: 835 Cloudnet - continuous evaluation of cloud profiles in seven operational models using ground-based observations, *Bull. Am. Meteorol. Soc.*, 88, 883-898, 2007.
- 645 Jossot, D., Pelon, J., Garnier, A., Hu, Y., Vaughan, M., Zhai, P.-W., Kuehn, R., and Lucker, P.: Cirrus optical depth and lidar ratio retrieval from combined CALIPSO-CloudSat observations using ocean surface echo, *J. Geophys. Res.*, 117, D05207, doi:10.1029/2011JD016959, 2012.
- 650 [Jylha](#), Kirsti & Tuomenvirta, Heikki & Ruosteenoja, Kimmo: Climate Change projections for Finland during the 21st century. *Boreal Environment Research*. 9, 2004.
- [Kienast-Sjogren](#), E., Rolf, C., Seifert, P., Krieger, U. K., Luo, B. P., [Kramer](#), M., and Peter, T.: Climatological and radiative properties of midlatitude cirrus clouds derived by automatic evaluation of lidar measurements, *Atmos. Chem. Phys.*, 16, 7605-7621, <https://doi.org/10.5194/acp-16-7605-2016>, 2016.
- 655 Klett, J. D.: Stable analytical inversion solution for processing lidar returns, *Appl. Opt.*, 20, [211-220](#), <https://doi.org/10.1364/AO.20.000211>, 1981.
- Kulmala, M., Asmi, A., Lappalainen, H. K., [Baltensperger, U.](#), [Brennguier, J.-L.](#), [Facchini, M. C.](#), [Hansson, H.-C.](#), [Hov, O.](#), [O'Dowd, C. D.](#), [Poschl, U.](#), [Wiedensohler, A.](#), [Boers, R.](#), [Boucher, O.](#), [de Leeuw, G.](#), [Denier van der Gon, H. A. C.](#), [Feichter, J.](#), [Krejci, R.](#), [Laj, P.](#), [Lihavainen, H.](#), [Lohmann, U.](#), [McFiggans, G.](#), [Mentel, T.](#), [Pilinis, C.](#), [Riipinen, I.](#), [Schulz, M.](#), [Stohl, A.](#), [Swietlicki, E.](#), [Vignati, E.](#), [Alves, C.](#), [Amann, M.](#), [Ammann, M.](#), [Arabas, S.](#), [Artaxo, P.](#), [Baars, H.](#), [Beddows, D. C. S.](#), [Bergstrom, R.](#), [Beukes, J. P.](#), [Bilde, M.](#), [Burkhart, J. F.](#), [Canonaco, F.](#), [Clegg, S. L.](#), [Coe, H.](#), [Crumevrolle, S.](#), [D'Anna, B.](#), [Decesari, S.](#), [Gilardoni, S.](#), [Fischer, M.](#), [Fjaeraa, A. M.](#), [Fountoukis, C.](#), [George, C.](#), [Gomes, L.](#), [Halleran, P.](#), [Hamburger, T.](#), [Harrison, R. M.](#), [Herrmann, H.](#), [Hoffmann, T.](#), [Hoose, C.](#), [Hu, M.](#), [Hyvarinen, A.](#), [Horrak, U.](#), [Iinuma, Y.](#), [Iversen, T.](#), [Josipovic, M.](#), [Kanakidou, M.](#), [Kiendler-Scharr, A.](#), [Kirkevåg, A.](#), [Kiss, G.](#), [Klimont, Z.](#), [Kolmonen, P.](#), [Komppula, M.](#), [Kristjansson, J.-E.](#), [Laakso, L.](#), [Laaksonen, A.](#), [Labonnote, L.](#), [Lanz, V. A.](#), [Lehtinen, K. E. J.](#), [Rizzo, L. V.](#), [Makkonen, R.](#), [Manninen, H. E.](#), [McMeeking, G.](#), [Merikanto, J.](#), [Minikin, A.](#), [Mirmo, S.](#), [Morgan, W. T.](#), [Nemitz, E.](#), [O'Donnell, D.](#), [Panwar, T. S.](#), [Pawlowska, H.](#), [Petzold, A.](#), [Pienaar, J. J.](#), [Pio, C.](#), [Plass-Duelmer, C.](#), [Prevot, A. S. H.](#), [Pryor, S.](#), [Reddington, C. L.](#), [Roberts, G.](#), [Rosenfeld, D.](#), [Schwarz, J.](#), [Seland, O.](#), [Sellegrì, K.](#), [Shen, X. J.](#), [Shiraiwa, M.](#), [Siebert, H.](#), [Sierau, B.](#), [Simpson, D.](#), [Sun, J. Y.](#), [Topping, D.](#), [Tunved, P.](#), [Vaattovaara, P.](#), [Vakkari, V.](#), [Veefkind, J. P.](#), [Visschedijk, A.](#), [Vuollekoski, H.](#), [Vuolo, R.](#), [Wehner, B.](#), [Wildt, J.](#), [Woodward, S.](#), [Worsnop, D. R.](#), [van Zadelhoff, G.-J.](#), [Zardini, A. A.](#), [Zhang, K.](#), [van Zyl, P. G.](#), [Kerminen, V.-M.](#), [Carslaw, K.](#), and [Pandis, S. N.](#): General overview: European Integrated project on Aerosol Cloud Climate and Air Quality [interaction-interactions](#) (EUCAARI) - integrating aerosol research from nano to global scales, *Atmos. Chem. Phys.*, 11, 13061-13143, [doi:https://doi.org/10.5194/acp-11-13061-2011](https://doi.org/10.5194/acp-11-13061-2011), 2011.
- 660 [Komppula, M.](#), [Mielonen, T.](#), [Arola, A.](#), [Korhonen, K.](#), [Lihavainen, H.](#), [Hyvarinen](#), A.-P., [Baars, H.](#), [Engelmann, R.](#), [Althausen, D.](#), [Ansmann, A.](#), [Muller](#), D., [Panwar, T. S.](#), [Hooda, R. K.](#), [Sharma, V. P.](#), [Kerminen, V.-M.](#), [Lehtinen, K. E. J.](#), and [Viisanen,](#)
- 670

- Y.: Technical Note: One year of Raman-lidar measurements in Gual Pahari EUCAARI site close to New Delhi in India [?](#). Seasonal characteristics of the aerosol vertical structure, *Atmos. Chem. Phys.*, 12, 4513-4524, <https://doi.org/10.5194/acp-12-4513-2012>, 2012.
- 675 Laakso, L., Vakkari, V., Virkkula, A., Laakso, H., Backman, J., Kulmala, M., Beukes, J. P., van Zyl, P. G., Tiitta, P., Josipovic, M., Pienaar, J. J., Chiloane, K., Gilardoni, S., Vignati, E., Wiedensohler, A., Tuch, T., Birmili, W., Piketh, S., Collett, K., Fourie, G. D., Komppula, M., Lihavainen, H., de Leeuw, G., and Kerminen, V.-M.: South African EUCAARI measurements: seasonal variation of trace gases and aerosol optical properties, *Atmos. Chem. Phys.*, 12, 1847-1864, <https://doi.org/10.5194/acp-12-1847-2012>, 2012.
- 680 Lakkis S. Gabriela, Lavorato Mario, Canziani Pablo, Lacomí Hector, Lidar observations of cirrus clouds in Buenos Aires, *Journal of Atmospheric and Solar-Terrestrial Physics*, Volumes [130-131](#), Pages 89-95, ISSN 1364-6826, <https://doi.org/10.1016/j.jastp.2015.05.020>. (<http://www.sciencedirect.com/science/article/pii/S1364682615001194>), 2015.
- Liou, K. N.: Influence of cirrus clouds on weather and climate processes: A global perspective, *Mon. Weather Rev.*, 114, [1167-1199](#), 1986.
- 685 Liu, J. J., Z. Q. Li, Y. F. Zheng, and M. Cribb: Cloud-base distribution and cirrus properties based on micropulse lidar measurements at a site in southeastern China. *Adv. Atmos. Sci.*, 32(7), [991-1004](#), doi: 10.1007/s00376-014-4176-2, 2015.
- Lynch D. K., Sassen K., Starr D.O'C. and Stephens G.: Cirrus, ISBN: 9780195130720.
- Martins, E., Noel V., and Chepfer H., Properties of cirrus and subvisible cirrus from nighttime Cloud-Aerosol Lidar with Orthogonal Polarization (CALIOP), related to atmospheric dynamics and water vapor, *J. Geophys. Res.*, 116, D02208, doi:10.1029/2010JD014519,
- 690 2011.
- Min, M., P. Wang, J. R. Campbell, X. Zong, and J. Xia: Cirrus cloud macrophysical and optical properties over north China from CALIOP measurements. *Adv. Atmos. Sci.*, 28(3), [653-664](#), doi: 10.1007/s00376-010-0049-5, 2011.
- [Noel, Vincent & Chepfer, Helene & Ledanois, Guy & Delaval, Arnaud & Flamant, Pierre.: Classification of Particle Effective Shape Ratios in Cirrus Clouds Based on the Lidar Depolarization Ratio. *Applied optics*. 41. 4245-57. 10.1364/AO.41.004245. 2002.](#)
- 695 Pandit, A. K., Gadhavi, H. S., Venkat Ratnam, M., Raghunath, K., Rao, S. V. B., and Jayaraman, A.: Long-term trend analysis and climatology of tropical cirrus clouds using 16 years of lidar data set over Southern India, *Atmos. Chem. Phys.*, 15, 13833-13848, <https://doi.org/10.5194/acp-15-13833-2015>, 2015.
- Platt, C. M. R.: Remote sounding of high clouds. III: Monte Carlo calculations of multiple scattered lidar returns, *J. Atmos. Sci.*, 38, [156-167](#), 1981.
- 700 [Reagan, J. A., X. Wang, and M. T. Osborn, Spaceborne lidar calibration from cirrus and molecular backscatter returns, *IEEE Trans. Geosci. Remote Sens.*, 40, 2285-2290, 2002.](#)
- Reichardt, J.: Optical and geometrical properties of northern midlatitude cirrus clouds observed with a UV Raman lidar. *Phys. Chem. Earth, Part B*, 24, [255-260](#), 1999.
- Ross, K. E., Piketh, S. J., Bruintjes, R. T., Burger, R. P., Swap, R. J., and Annegarn, H. J.: Spatial and seasonal variations in CCN distribution and the aerosol-CCN relationship over southern Africa, *J. Geophys. Res.*, 108, 8481, doi:10.1029/2002JD002384, 2003.
- 705 Sassen, K. and S. Benson, 2001: A Midlatitude Cirrus Cloud Climatology from the Facility for Atmospheric Remote Sensing. Part II: Microphysical Properties Derived from Lidar Depolarization. *J. Atmos. Sci.*, 58, [2103-2112](#), [https://doi.org/10.1175/1520-0469\(2001\)058<2103:AMCCCF>2.0.CO;2](https://doi.org/10.1175/1520-0469(2001)058<2103:AMCCCF>2.0.CO;2), 2001.
- Sassen, K. and Cho, B. S.: Subvisual-Thin cirrus lidar dataset for satellite verification and climatological research, *J. Appl. Meteorol.*, 31, [1275-1285](#), doi:10.1175/1520-0450(1992)031<1275:STCLDF>2.0.CO 2 , 1992.
- 710

- Sassen, K., Z. Wang, and D. Liu, Global distribution of cirrus clouds from CloudSat/Cloud-Aerosol Lidar and Infrared Pathfinder Satellite Observations (CALIPSO) measurements, *J. Geophys. Res.*, 113, D00A12, doi:10.1029/2008JD009972, 2008.
- Seifert, P., Ansmann, A., Muller, D., Wandinger, U., Althausen, D., Heymsfield, A. J., Massie, S. T., and Schmitt C.: Cirrus optical properties observed with lidar, radiosonde, and satellite over the tropical Indian Ocean during the aerosol-polluted northeast and clean maritime southwest monsoon, *J. Geophys. Res.*, 112, D17205, doi:10.1029/2006JD008352, 2007.
- 715 [Vaughan, M. A., Liu, Z., McGill, M. J., Hu, Y., and Obland, M. D.: On the spectral dependence of backscatter from cirrus clouds: Assessing CALIOP's 1064 nm calibration assumptions using cloud physics lidar measurements, *J. Geophys. Res.*, 115, D14206, doi:10.1029/2009JD013086, 2010.](#)
- Wandinger, U.: Multiple-scattering influence on extinction- and backscatter-coefficient measurements with Raman and high-spectral resolution lidars, *Appl. Opt.*, 37, ~~417-427~~417-427, 1998.
- 720 [Westbrook, C. D., and Illingworth, A. J.: Evidence that ice forms primarily in supercooled liquid clouds at temperatures > -27°C, *Geophys. Res. Lett.*, 38, L14808, doi:10.1029/2011GL048021, 2011.](#)
- Young, S. A. and Vaughan, M. A.: The Retrieval of Profiles of Particulate Extinction from Cloud-Aerosol Lidar Infrared Pathfinder Satellite Observations (CALIPSO) Data: Algorithm Description, *J. Atmospheric Ocean. Technol.*, 26, ~~1105-1119~~1105-1119,doi:10.1175/2008JTECHA1221.1, 2009.
- 725 Young, S. A., Vaughan, M. A., Kuehn, R. E., and Winker, D. M.: The Retrieval of Profiles of Particulate Extinction from ~~Cloud-Aerosol~~ [Cloud-Aerosol](#) Lidar and Infrared Pathfinder Satellite Observations (CALIPSO) Data: Uncertainty and Error Sensitivity Analyses, *J. Atmospheric Ocean. Technol.*, 30, ~~395-428~~395-428, doi:10.1175/JTECH-D-12-00046.1, 2013.
- 730 [Young, S. A., Vaughan, M. A., Garnier, A., Tackett, J. L., Lambeth, J. D., and Powell, K. A.: Extinction and optical depth retrievals for CALIPSO's Version 4 data release, *Atmos. Meas. Tech.*, 11, 5701-5727, <https://doi.org/10.5194/amt-11-5701-2018>, 2018.](#)

Table 1. Technical specifications of the Polly^{XT} System.

Characteristics	Polly ^{XT}
Operating Wavelength(s)	355nm, 532nm, 1064nm
Average pulse energy	~450 mJ
Laser beam divergence	<0.2 mrad
Telescope diameter	0.3m
Receiver field of view	1mrad
Detectors	Hamamatsu PMTs
Polarization	Cross & Total
Raw data range resolution	30m
Raw data time resolution	30s

Table 2. ~~Number of detected cirrus layers, percentages of each Average cirrus category, mean values of Lidar Ratio and the particle depolarization properties~~ for the three regions ~~for daytime and nighttime measurements.~~

Station Cirrus Properties	<u>Gual Pahari</u>	<u>Elandsfontein</u>	<u>Kuopio</u>
<u>Cirrus Base (m)</u>	<u>8947 ± 1465</u>	<u>9200 ± 810</u>	<u>7969 ± 1080</u>
	<u>8900 ± 1480 d</u>	<u>9400 ± 818 d</u>	<u>7922 ± 914 d</u>
	<u>9000 ± 1229 n</u>	<u>9300 ± 744 n</u>	<u>8193 ± 1246 n</u>
<u>Cirrus Top (m)</u>	<u>10600 ± 1500</u>	<u>10826 ± 906</u>	<u>9280 ± 1075</u>
	<u>10550 ± 1453 d</u>	<u>10705 ± 928 d</u>	<u>8965 ± 1095 d</u>
	<u>10700 ± 1640 n</u>	<u>10889 ± 928 n</u>	<u>9443 ± 1055 n</u>
<u>Cirrus geometrical thickness (m)</u>	<u>1500 ± 489</u>	<u>1500 ± 735</u>	<u>1200 ± 585</u>
	<u>1480 ± 451 d</u>	<u>1527 ± 802 d</u>	<u>1157 ± 714 d</u>
	<u>1537 ± 638 n</u>	<u>1496 ± 616 n</u>	<u>1343 ± 456 n</u>
<u>Temperature base (C)</u>	<u>-33 ± 5</u>	<u>-34 ± 5</u>	<u>-43 ± 10</u>
<u>Temperature top (C)</u>	<u>-43 ± 5</u>	<u>-45 ± 6</u>	<u>-57 ± 9</u>

Table 3. Average cirrus optical properties for the three regions for daytime and nighttime measurements.

<u>Cirrus Properties</u>	<u>Gual Pahari</u>	<u>Elandsfontein</u>	<u>Kuopio</u>
N	<u>11 (7d, 4n)</u>	<u>64 (32d, 32n)</u>	<u>213 (153d, 50n)</u>
% subvisible	<u>0</u>	<u>2</u>	<u>3</u>
% thin	<u>28</u>	<u>53</u>	<u>71</u>
% opaque	<u>72</u>	<u>45</u>	<u>26</u>
LR 355	27 ± 12 22 ± 8 d 29 ± 7 n	26 ± 6 27 ± 5 d 26 ± 6 n	33 ± 7 33 ± 7 d 32 ± 7 n
LR 532	Particle depol 27 ± 16 22 ± 3 d 31 ± 11 n	25 ± 6 23 ± 5 d 25 ± 6 n	31 ± 7 30 ± 7 d 30 ± 7 n
Kuopio-COD 355	229 0.60 ± 0.40 0.46 ± 0.30 d 0.90 ± 0.40 n	3 0.35 ± 0.30 0.34 ± 0.30 d 0.36 ± 0.30 n	70 0.25 ± 0.20 0.25 ± 0.21 d 0.26 ± 0.16 n
<u>COD 532</u>	27 0.45 ± 0.35 0.40 ± 0.30 d 0.50 ± 0.40 n	0.3 ± 0.30 0.30 ± 0.30 d 0.30 ± 0.30 n	0.24 ± 0.19 0.29 ± 0.27 d 0.18 ± 0.10 n
<u>CR (355/532)</u>	<u>1.5 ± 0.8</u>	<u>1.4 ± 1.1</u>	<u>1.1 ± 0.9</u>

Table 4. Predominant aerosol type and AOD FT for the three regions.

<u>Measurement Site</u>	<u>Gual Pahari</u>	<u>Elandsfontein</u>	<u>Kuopio</u>
<u>Predominant aerosol type</u>	<u>dust particles , biomass burning</u>	<u>biomass burning, desert dust particles and urban particles</u>	<u>fine particles</u>
<u>AOD FT</u>	<u>0.09 ± 0.03</u>	<u>0.06 ± 0.04</u>	<u>0.006 ± 0.01</u>
<u>COD</u>	<u>0.60 ± 0.39</u>	<u>0.35 ± 0.30</u>	<u>0.25 ± 0.20</u>

Table 5. Summary of cirrus clouds geometrical and optical properties of ground-based lidar observations reported in literature.

<u>Measurement site</u>	<u>Location</u>	<u>Cirrus Base (km)</u>	<u>Cirrus Top (km)</u>	<u>LR (sr)</u>	<u>COD</u>	<u>R</u>
<u>Kuopio</u>	<u>62.74°N, 27.54°E</u>	<u>8.0 ± 1.1</u>	<u>9.5 ± 1.1</u>	<u>33 ± 7</u>	<u>0.25 ± 0.20</u>	<u>T</u>
<u>France</u>	<u>43.9°N, 5.7°E</u>	<u>9.3 ± 1.8</u>	<u>10.9 ± 1.7</u>			<u>Hoare</u>
<u>Rome</u>	<u>41.8°N, 12.6°E</u>			<u>31 ± 15</u>	<u>0.37 ± 0.18 (532nm)</u>	<u>Dioni</u>
<u>Thessaloniki</u>	<u>40.6°N, 22.9°E</u>	<u>8.8 ± 1.0</u>	<u>10.3 ± 0.9</u>	<u>30 ± 8-17</u>	<u>0.38-0.31 ± 0.24 (355nm)</u>	<u>Gianna</u>
<u>Gual Pahari-height Naqu</u>	<u>25-31.5°N, 92.1°E</u>	<u>0-13.7 ± 2</u>	<u>15.6 ± 1.6</u>	<u>28 ± 15</u>	<u>72-0.33 ± 0.29 (532nm)</u>	<u>He</u>
<u>Gual Pahari</u>	<u>28.43°N, 77.15°E</u>	<u>9.0 ± 1.5</u>	<u>10.6 ± 1.5</u>	<u>26±12</u>	<u>27-0.59 ± 16-0.39(355nm)</u>	<u>-T</u>
<u>Elandsfontein-height Gadanki</u>	<u>88-13.5°N, 79.2°E</u>	<u>4-13.0 ± 2.2</u>	<u>52-15.3 ± 2.0</u>	<u>44-</u>	<u>25-</u>	<u>Pandi</u>
<u>Hulule</u>	<u>4.1°N, 73.3°E</u>	<u>12 ± 6-1.6</u>	<u>24-13.7 ± 1.4</u>	<u>32</u>	<u>0.28 (532nm)</u>	<u>Seifer</u>
<u>Amazonia</u>	<u>2.89°S, 59.97°W</u>	<u>12.9 ± 2</u>	<u>14.3 ± 1.9</u>	<u>23 ± 8</u>	<u>0.25 ± 0.46 (355nm)</u>	<u>Gouve</u>
<u>La Reunion</u>	<u>20.8°S, 55.5°W</u>		<u>13.0</u>		<u>0.05</u>	<u>Hoare</u>
<u>Elandsfontein</u>	<u>26.25°S, 29.43°E</u>	<u>9.2 ± 0.8</u>	<u>11 ± 0.9</u>	<u>26 ± 6</u>	<u>-0.35 ± 0.30</u>	<u>T</u>
<u>Buenos Aires</u>	<u>34.6°S, 58.5°W</u>	<u>9.6</u>	<u>11.8</u>		<u>0.26 ± 0.11</u>	<u>Lakki</u>

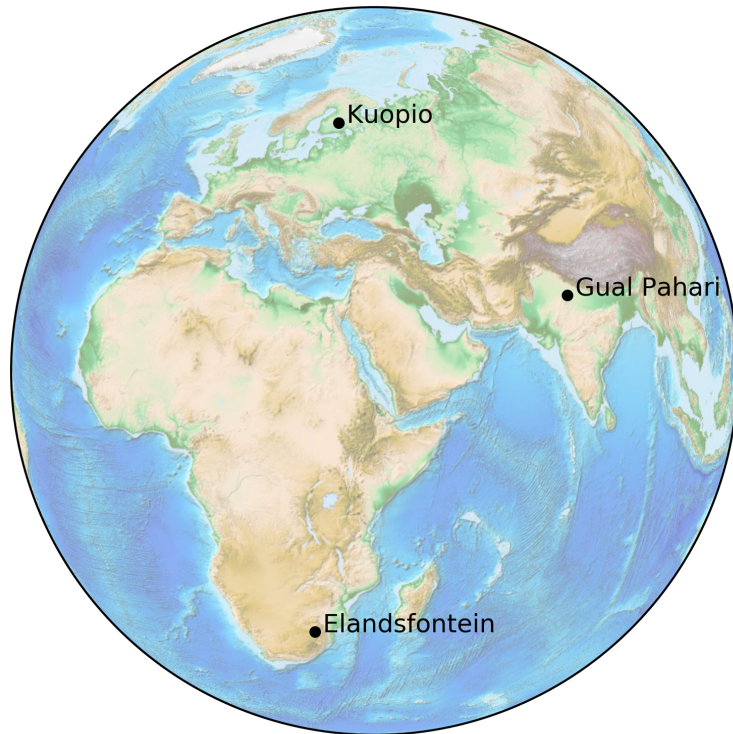


Figure 1. [Map of the three measuring sites.](#)

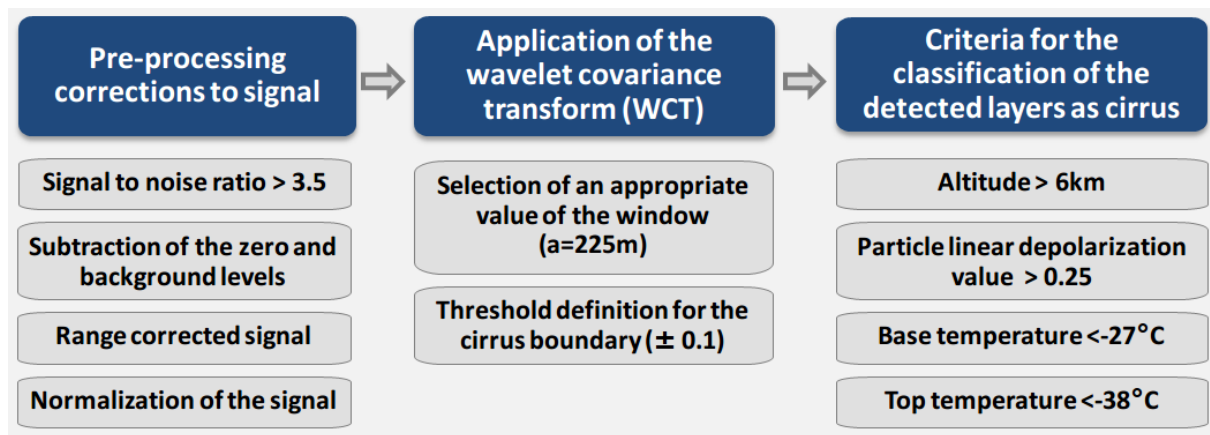


Figure 2. Schematic flowchart showing the main steps of the methodology applied in this study to obtain the cirrus geometrical boundaries from the Polly^{XT} measurements.

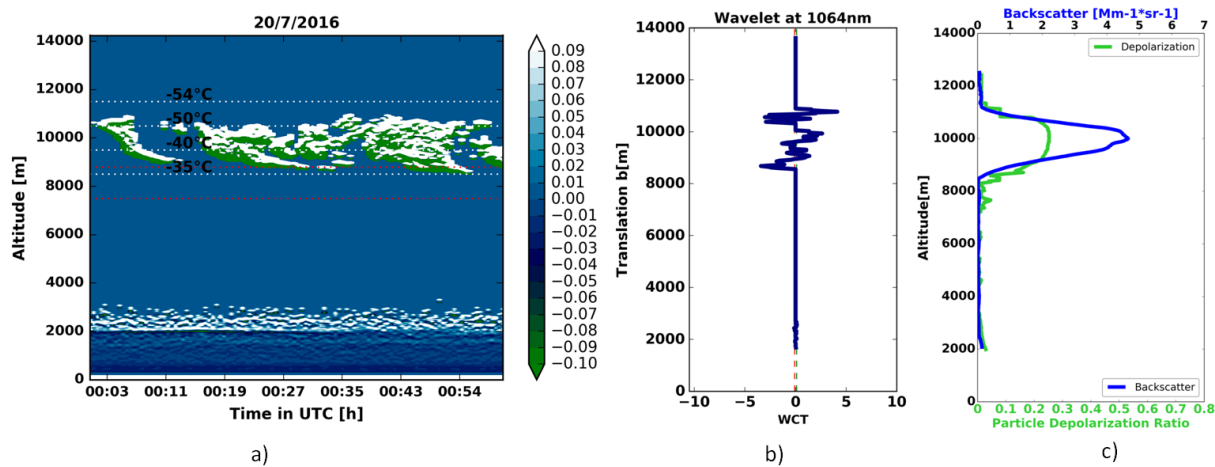


Figure 3. Cirrus cloud evolution as determined from the Polly^{XT} observations for 1 hour observation with temperatures marked with white lines and the temperatures criteria marked with red lines (a), the 1-hour averaged wavelet applied to the corrected 1064 signal (b) and the hourly mean particle Depolarization ratio for the whole period of study (green) and backscatter coefficient (blue) at 532nm (c) on 20th of July 2016 at Kuopio station.

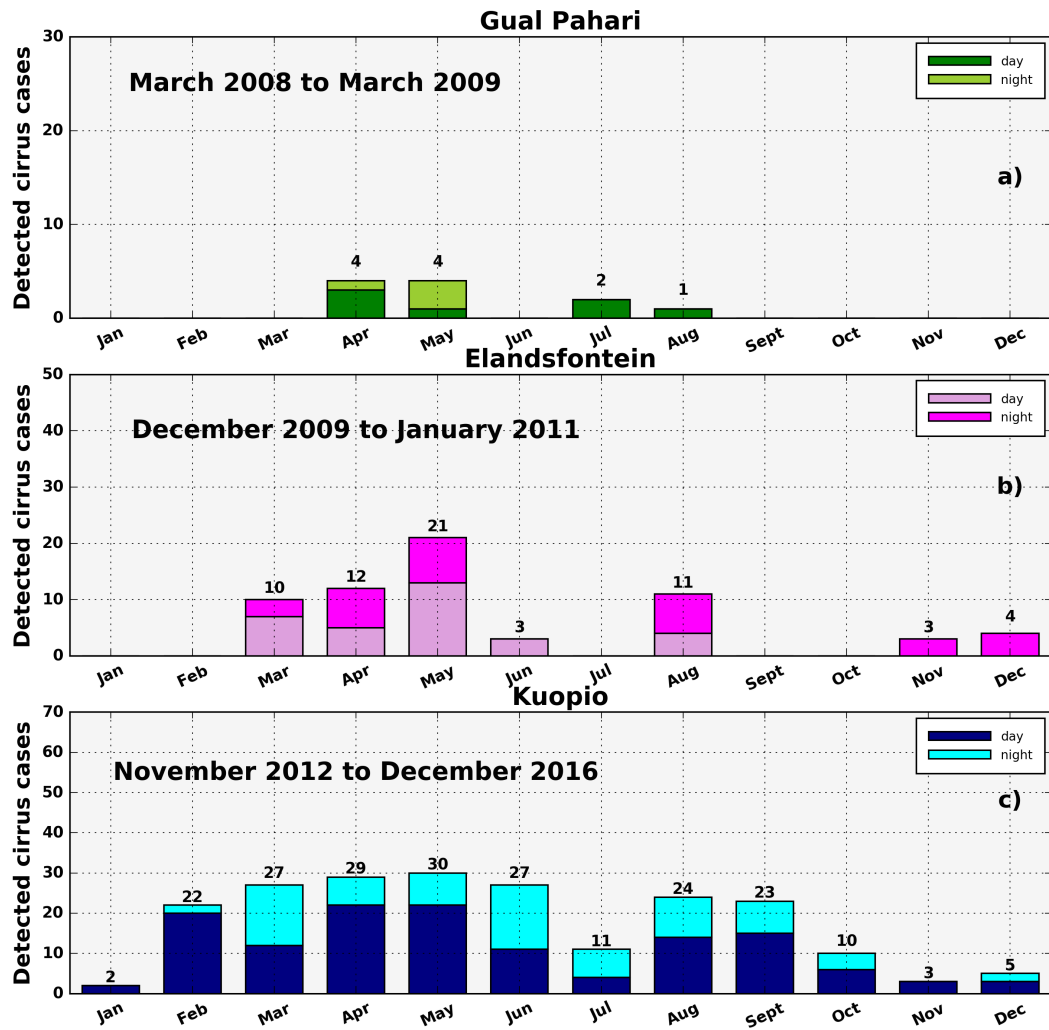


Figure 4. Cirrus detection with the Polly^{XT} over Gual Pahari, India during the period 2008-2009 (a) Elandsfontein, South Africa during the period 2009-2010(b) and Kuopio (c), Finland during 2014-2016.

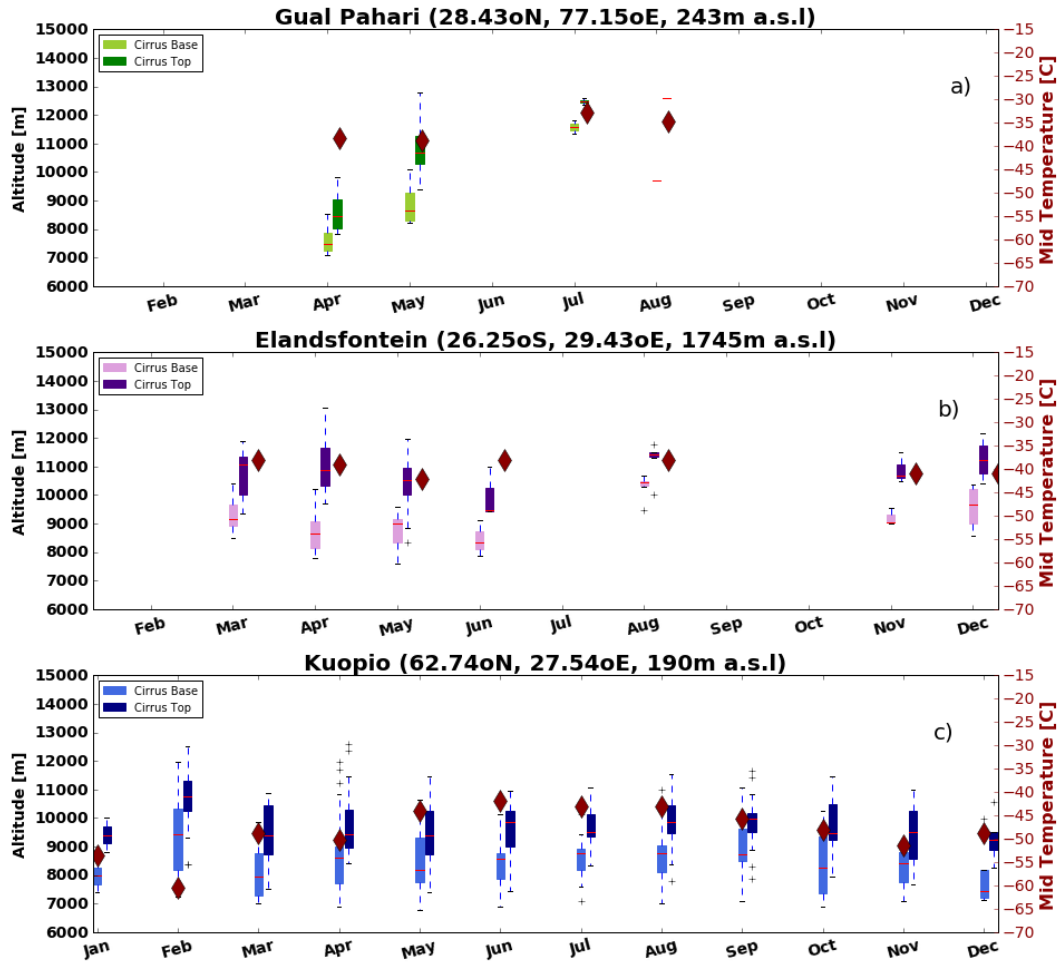


Figure 5. Monthly cycle of mean base, mean top and the corresponding temperature base values (circles) of the cirrus clouds at Kuopio (a), Gual Pahari (b) and Elandsfontein (c). Horizontal line in box: median. Boxes: the upper and lower quartile. Whisker: extreme values.

Histograms of (a) the COD at 355nm, (b) the COD at 532nm, (c) the Lidar Ratio at 355nm and (d) the Lidar Ratio at 532nm of the cirrus detected layers observed over Kuopio, Finland:

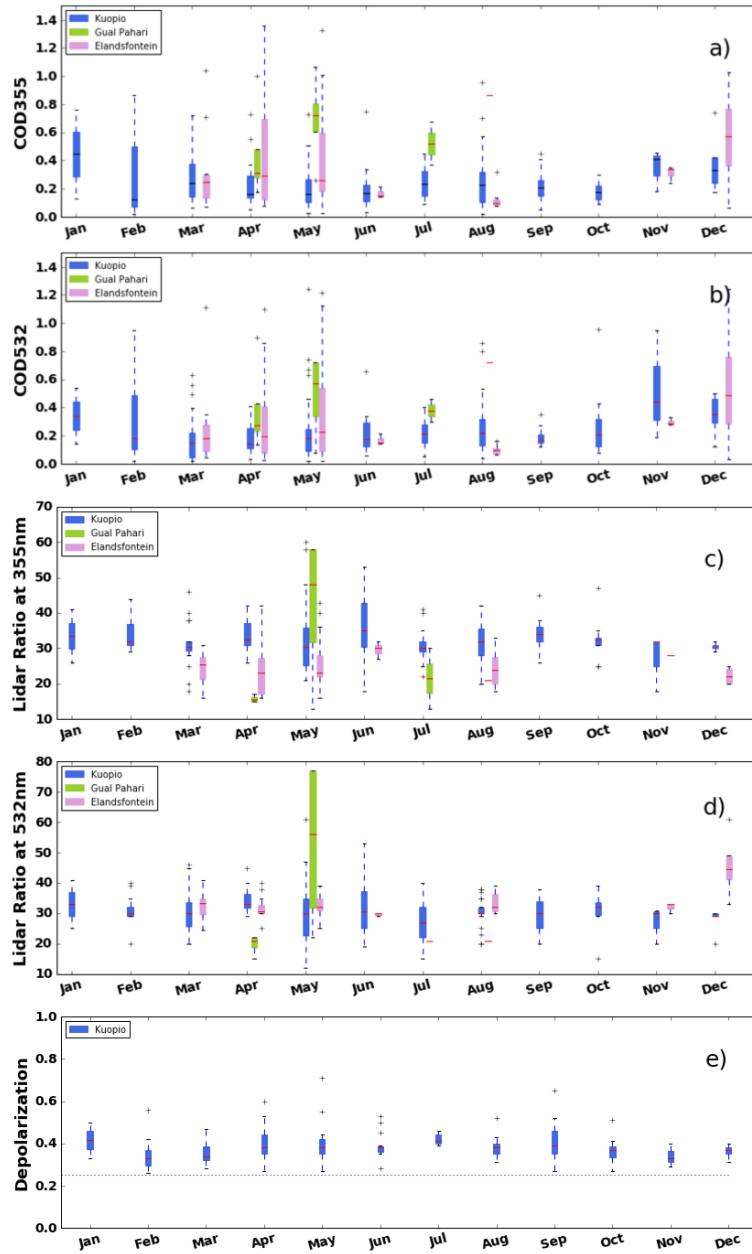


Figure 6. (a) Mean optical depth (multiple scattering corrected) values at 355nm, (b) mean optical depth (multiple scattering corrected) values at 532nm, (c) Lidar Ratio-ratio at 355nm, (d) Lidar Ratio-ratio at 532nm and (e) particle depolarization ratio for the detected cirrus layers for the study period of the three regions. Horizontal line in box: median. Boxes: the upper and lower quartile. Whisker: extreme values. Red line stands for the mean values for every month.

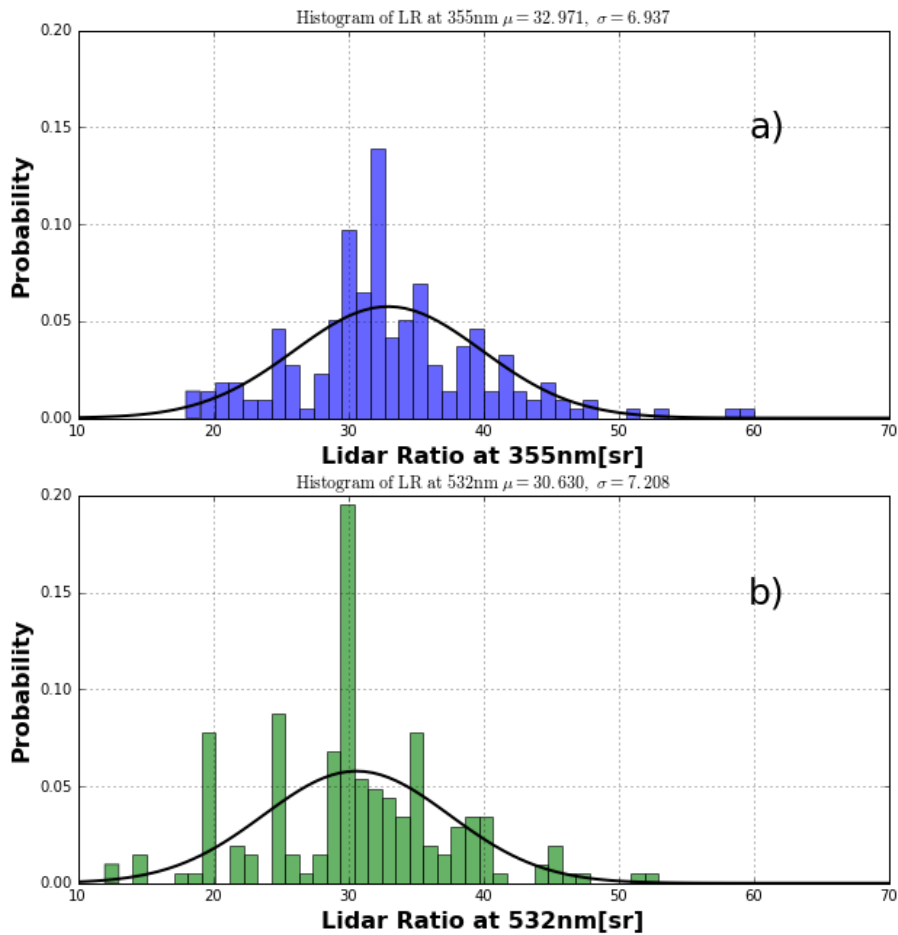


Figure 7. Histograms of (a) the Lidar ratio at 355nm and (b) the Lidar ratio at 532nm of the cirrus detected layers observed over Kuopio, Finland.

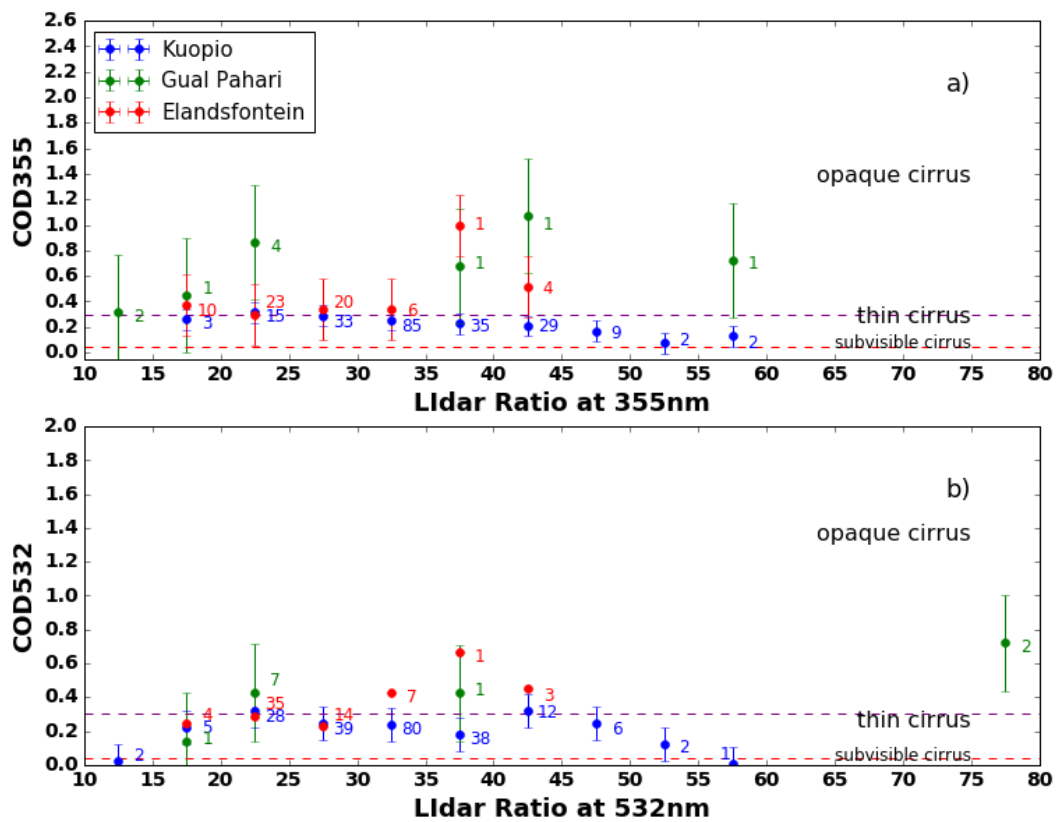


Figure 8. Dependence of (a) the corrected lidar ratio with COD at 355nm and (b) the corrected lidar ratio with COD at 532nm. Numbers labeled indicate the number of cases per lidar ratio bin. Horizontal dashed lines: cirrus categories by Sassen and Cho (1992).

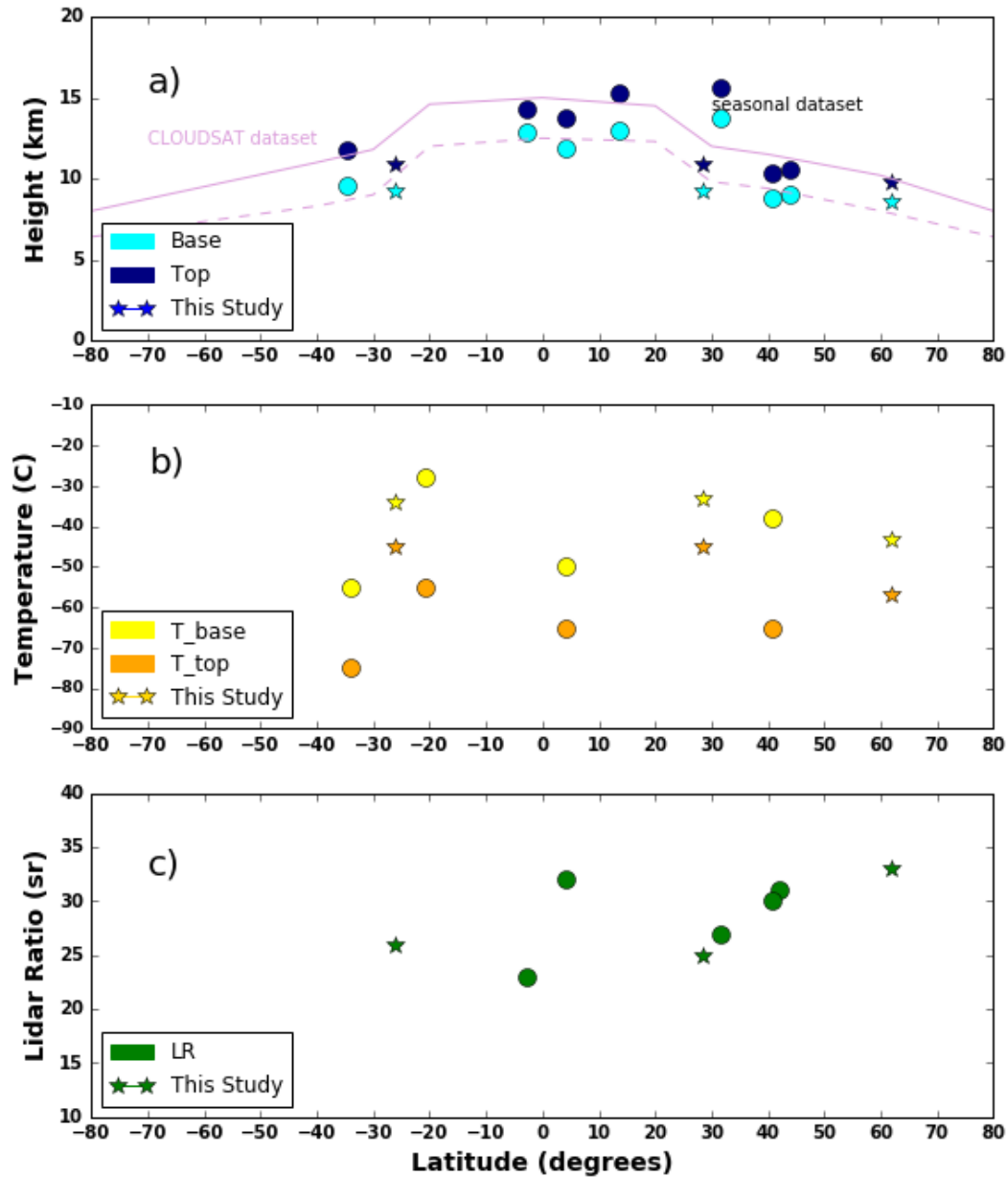


Figure 9. Latitudinal dependence of cirrus base and top height. Circles denote estimations from groundbased lidar from the literature (see Table 5 for references), stars denote estimations from this study and lines correspond to CLOUDSAT estimations according to Sassen et al. (2008) (a), latitudinal dependence of cirrus temperature base and top. Circles denote estimations from groundbased lidar from the literature (see Table 5 for references), stars denote estimations from this study and (b) same as above, but for latitudinal dependence of lidar ratio values (c).

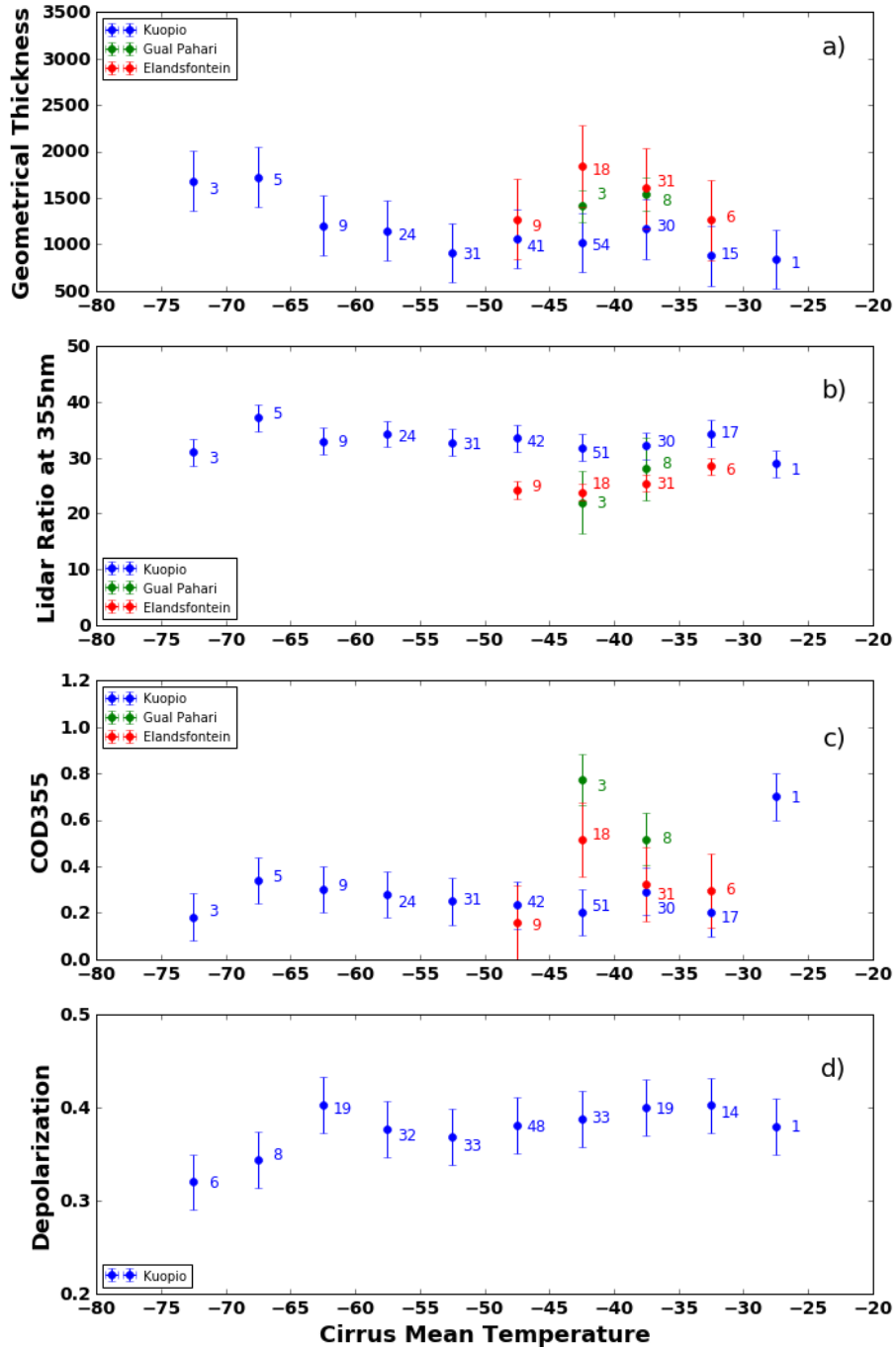


Figure 10. Dependencies of (a) geometrical thickness, (b) lidar ratio, (c) optical depth at 355nm and (d) particle depolarization values on 5°C intervals of cirrus base-mid temperature. Numbers labeled indicate the number of cases per temperature bin.

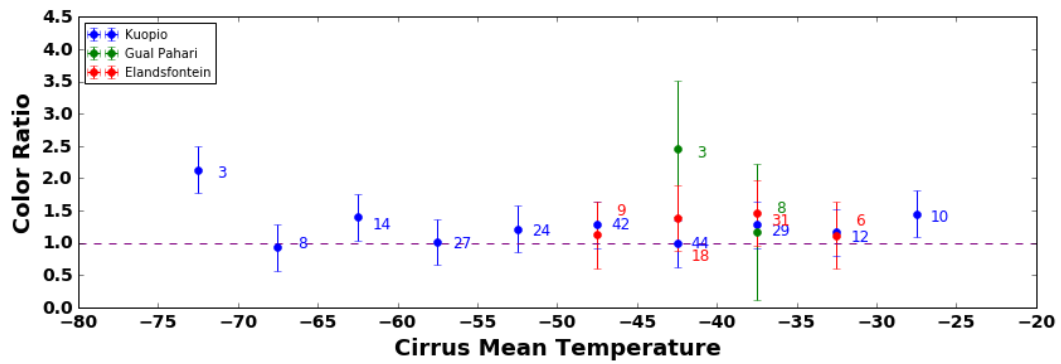


Figure 11. Dependencies of color ratio (355/532) on 5°C intervals of cirrus mid temperature. Numbers labeled indicate the number of cases per temperature bin.

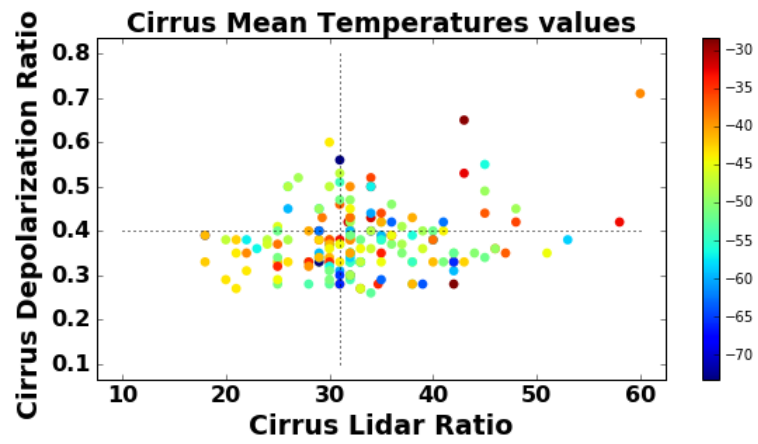


Figure 12. [Dependencies of the mean temperature with the Lidar ratio values at 355nm and the particle depolarization values.](#)